

Impacts of high precipitation on the energy and water budgets of a humid boreal forest

Pierre-Erik Isabelle ^{a,b}, Daniel F. Nadeau ^{a,b,*}, François Anctil ^{a,b}, Alain N. Rousseau ^d, Sylvain Jutras ^{a,c}, Biljana Music ^e

^a *CentrEau - Water Research Center, Université Laval, 1065 avenue de la Médecine, Québec, QC, Canada.*

^b *Department of Civil and Water Engineering, Université Laval, 1065 avenue de la Médecine, Québec, QC, Canada.*

^c *Department of Forestry and Wood Science, Université Laval, 2405 rue de la Terrasse, Québec, QC, Canada.*

^d *Institut national de la recherche scientifique - Centre Eau Terre Environnement, 490 rue de la Couronne, Québec, QC, Canada.*

^e *Ouranos Consortium, 550 Sherbrooke St West, Montréal, QC, Canada*

Abstract

The boreal forest will be strongly affected by climate change and in turn, these vast ecosystems may significantly impact global climatology and hydrology due to their exchanges of carbon and water with the atmosphere. It is now crucial to understand the intricate relationships between precipitation and evapotranspiration in these environments, particularly in less-studied locations characterized by a cold and humid climate. This study presents state-of-the-art measurements of energy and water budgets components over three years (2016-2018) at the Montmorency Forest, Québec, Canada: a balsam fir boreal forest that receives ~1600 mm of precipitation annually (continental subarctic climate; Köppen classification subtype Dfc). Precipitation, evapotranspiration and potential evapotranspiration at the site are compared with observations from thirteen experimental sites around the world. These intercomparison sites (89 study-years) encompass various types of climate and vegetation (black spruces, jack pines, etc.) encountered in boreal forests worldwide. The Montmorency Forest stands out by receiving the largest amount of precipitation. Across all sites, water availability seems to be the principal evapotranspiration constraint, as precipitation tends to be more influential than potential evapotranspiration and other factors. This leads to the Montmorency Forest generating the largest amount of evapotranspiration, on average ~550 mm y⁻¹. This value appears to be an ecosystem maximum for evapotranspiration, which may be explained either by a physiological limit or a limited energy availability due to the presence of cloud cover. The Montmorency Forest water budget evacuates the precipitation excess mostly by watershed discharges, at an average rate of ~1050 mm y⁻¹, with peaks during the spring freshet. This behaviour, typical of mountainous headwater basins, necessarily influence downstream hydrological regimes to a large extent. This study provides a much needed insight in the hydrological regimes of a humid boreal-forested mountainous watershed, a type of basin rarely studied with precise energy and water budgets before.

Keywords: Evapotranspiration; Energy Budget; Boreal Forest; Water Budget; Watershed Hydrology; Eddy-Covariance

37 **1. Introduction**

38 The boreal forest covers roughly 14% of the Earth emerged surface, globally enclosing 30% of
39 the world's forests (Brandt et al., 2013; Gauthier et al., 2015). It is the second largest vegetated area in
40 extent (12 to 14 million km²) behind tropical forests (Landsberg & Gower, 1997). Furthermore, it
41 sequesters 20% of the global forest carbon (Pan et al., 2011). On the whole, the circumpolar boreal
42 biome controls fluxes of carbon and water over a huge area and thus impacts the Earth's global
43 climatology and hydrology. In return, global climate tremendously affects the boreal forest; this biome
44 will in all likelihood experience one of the strongest warming in the future (IPCC, 2013), lengthening
45 the growing season and forest productivity (Kauppi et al., 2014; Schaphoff et al., 2016; Liu et al., 2019).
46 In some regions, these changes could be modulated by lower precipitation leading to conditions where
47 evapotranspiration is unable to meet an increase in evaporative demand (Barber et al., 2000; Lloyd &
48 Bunn, 2007; Walker et al., 2015). However, boreal forest regions of northeastern North America,
49 enduring large precipitation, could be sheltered from such destructive effects (D'Orangeville et al.,
50 2016).

51 For these reasons, there is a need to further our understanding of the intricate relationship
52 between precipitation (P), evapotranspiration (E), and evaporative demand in various regions of the
53 boreal forest. The first step towards this goal is to quantify the energy and water budgets of the
54 ecosystem.

55 The surface energy budget of for a watershed covered by forest can be described as follows:

56

$$57 R_n = H + \lambda E + G + \Delta Q \quad (1)$$

58

59 where R_n is the net radiation; H , the sensible heat flux; λE , the latent heat flux associated with
60 evaporation of surface water and transpiration of vegetation, or evapotranspiration; G , the soil heat
61 flux; ΔQ , variations in storage of heat in the air and biomass below a certain height – all terms are
62 expressed as energy fluxes per surface area in $W\ m^{-2}$.

63 Similarly, the water budget of a watershed can be described as:

64

$$65 P = E + O + \Delta S \quad (2)$$

66

67 where P is the total precipitation; E , the evapotranspiration; O , the watershed outflow, in streams and
68 grounds; ΔS , the storage variations of water in the ground via water table and soil water content
69 fluctuations and above the ground via snowpack accumulation – with all terms are expressed in mm;
70 that is for a given time interval as water volumes per surface area of the watershed. In both budgets,
71 the left-side terms are input of energy or water, while right-side terms generally express outputs. E is
72 the obvious link between energy and water budgets, appearing in both Equations (1) and (2) (as a

73 mass flux in the former and as a water height in the second, the latter being the mass flux multiplied
74 by the time interval over water density).

75 The boreal forest energy budget has been documented at length during the Boreal Ecosystem
76 Atmosphere Study (BOREAS; Sellers et al., 1995; 1997) and in the ensuing measurement years at the
77 Boreal Ecosystem Research and Monitoring Sites (BERMS; Barr et al., 2002). The mostly evergreen
78 canopy absorbs a large amount of solar radiation year-long (Sellers et al., 1997). In the BERMS studied
79 area, the absorbed energy returns to the atmosphere mostly by means of H (Saugier et al., 1997; Barr
80 et al., 2001; Coursolle et al., 2006; Gao et al., 2017), except in the presence of deciduous species
81 (Blanken et al., 1997; Zha et al., 2010; Brown et al., 2014). The incidentally low E rates still account for
82 a large portion of annual P , leaving small volumes to generate watershed outflows (Nijssen &
83 Lettenmaier, 2002; Barr et al., 2012). Similar results were also observed in Scandinavia (Ilvesniemi et
84 al., 2010) and Russia (Oltchev et al., 2002).

85 Because of their climate, the aforementioned BERMS sites cannot effectively describe the
86 effects of high rainfall on the energy and water budgets of the boreal forest. While the humid forests of
87 northeastern North America have been studied for their carbon budget (Giasson et al., 2006; Bergeron
88 et al., 2007; Payeur-Poirier et al., 2012), a detailed description of the interrelationships between the
89 energy and water budgets is still lacking. Besides, very few studies have used precise E measurements
90 to assess the water balance of the boreal forest at the watershed scale (*e.g.*, Nijssen & Lettenmaier,
91 2002; Ilvesniemi et al., 2010; Barr et al., 2012), none in precipitation-heavy regions, to the best of our
92 knowledge. Given that these regions are expected to undergo changing climate conditions, more
93 studies are needed.

94 This work assesses the impacts of high precipitation on boreal forest energy and water
95 budgets for the balsam fir – white birch bioclimatic domain. The experimental site is a small watershed
96 featuring an extensive instrumental setup measuring most terms of the energy and water budgets. The
97 watershed, at the southern extent of the circumpolar boreal biome, is subject to particularly high
98 precipitation, making it an ideal site for this study. This paper is specifically interested in: (i) comparing
99 the energy and vertical water budgets of the main study site and specifically E - P interactions with
100 observed values in other boreal forest sites around the world; and (ii) quantify the impact of E - P
101 interactions on the water budget, specifically on measured discharges. Results are based on three-year
102 flux tower measurements in two locations featuring trees at different stages of maturity. Comparison
103 data include 89 study-years spread over 13 sites around the circumpolar boreal biome.

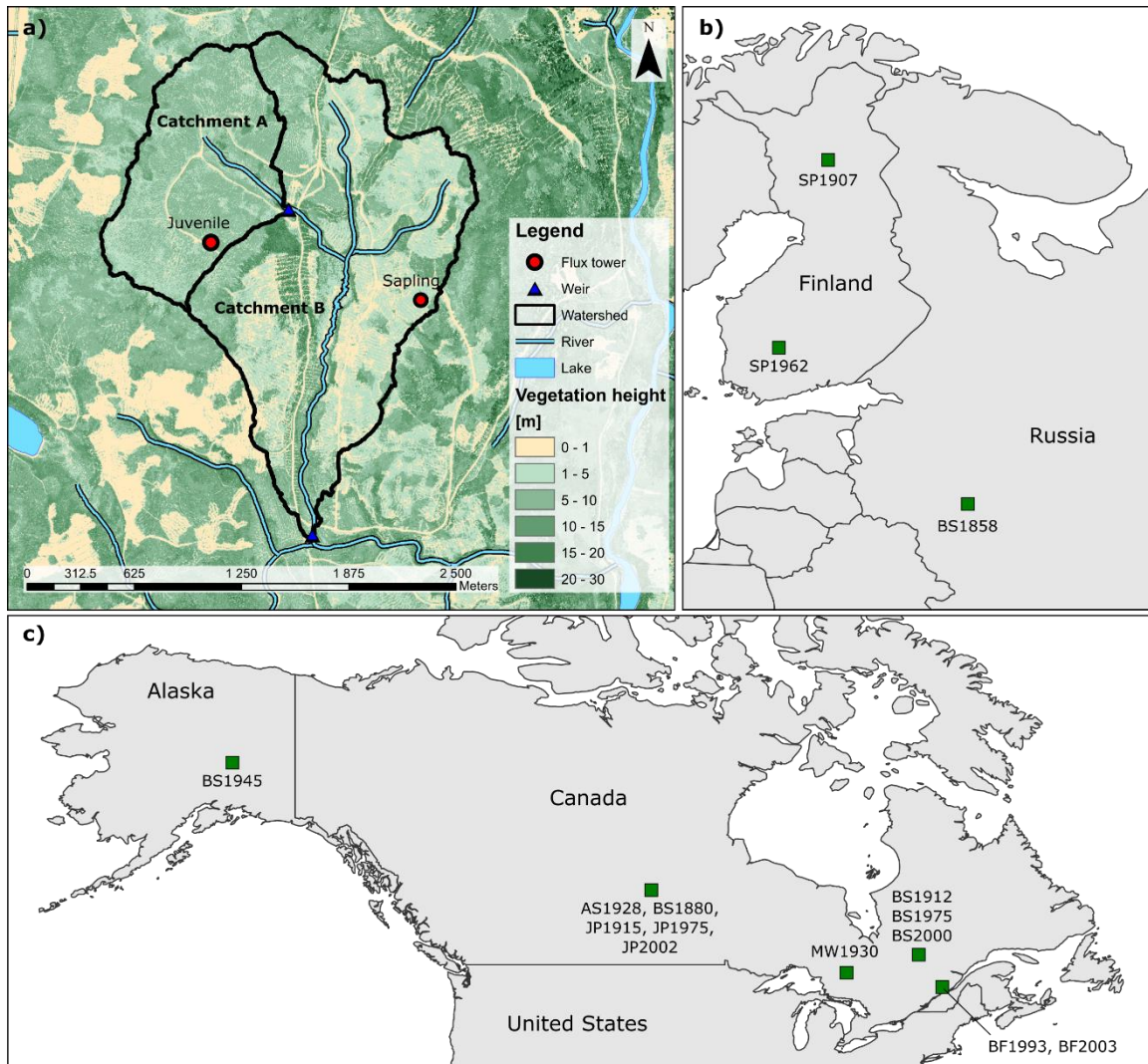
104

105 **2. Main Study Site**

106 *2.1. Site description*

107 The main study site is located in the Montmorency Forest (47°17'18"N; 71°10'05.4"W), 80 km
108 north of Québec City, Canada (BF1993 and BF2003 in Figure 1c), part of the balsam fir – white birch

109 bioclimatic domain. Specifically, two flux towers were installed in the “Bassin Expérimental du
 110 Ruisseau des Eaux-Volées” (BEREV) (Lavigne, 2007; Tremblay et al., 2008, 2009; Noël et al., 2014;
 111 Isabelle et al., 2018a). This experimental watershed lies at a mean altitude of 750 m above mean sea
 112 level (AMSL) with peaks at 1000 m AMSL. Figure 1a presents the boundaries of two sub-catchments of
 113 the BEREV covering an area of 3.6 km². The sub-catchment A, located upstream of the sub-catchment
 114 B, is gauged and has a 1.2-km² area; the sub-catchment B, which is also gauged, has a 2.4-km² area. The
 115 general slope of the entire catchment, referred to here as AB, is 0.064 m m⁻¹.
 116



117

118 Figure 1: a) Location of instruments at the study site, with catchment boundaries and vegetation height from LiDAR surveys
 119 (Source: Ministère Forêts, Faune et Parcs du Québec); b) Location of European study sites; c) Location of study sites in North
 120 America.

121 The vegetation of both catchments consists mostly of balsam fir (*Abies balsamea* (L.) Mill)
122 along white birch (*Betula papyrifera* Marsh) and white spruce (*Picea glauca* (Moench) Voss) (Lavigne,
123 2007; Tremblay et al., 2008, 2009). Trees reach heights between 4-8 m in the sub-catchment A, the
124 product of natural regeneration after the logging of 85% of the trees in 1993. The trees are labeled as
125 “juvenile”, hence the flux tower name. Sub-catchment B was logged progressively between 2000 and
126 2010, but not entirely. Tree height distribution is heterogeneous, but in the vicinity of the flux tower
127 prevails trees 2-4 m tall that was classified as “sapling”, hence naming the flux tower.

128 The Montmorency Forest is under the influence of a continental subarctic climate (Köppen
129 classification subtype Dfc) with a short and cool growing season and high volumes of year-round
130 precipitation. Mean annual temperature is 0.5°C and mean annual precipitation amounts to 1583 mm
131 (40% as snow) over the period of 1981-2010, as per Environment and Climate Change Canada (Station
132 “Foret Montmorency”, available at:
133 http://climat.meteo.gc.ca/historical_data/search_historic_data_f.html).

134

135 2.2. Instrumental setup

136 Two flux towers were installed in the BEREV in October 2015: the Juvenile and Sapling flux
137 towers (see Figure 1a). The Juvenile flux tower is a 15-m scaffolding structure featuring two sets of
138 sonic anemometers and CO₂/H₂O gas analyzers (IRGASONS, Campbell Scientific, USA). The two devices
139 are mounted 14.63 m above the ground, or ≈8 m above the top of the canopy, and face opposite
140 directions (303°, northwest; and 118°, southeast). This feature allows for optimal flux quality control,
141 since wind interference by the tower structure and devices is avoided by combining both time series
142 based on wind direction. Both devices were installed parallel to the local 12° northeast-facing slope.
143 This alignment is required to apply the eddy-covariance method on sloped terrain (Turnipseed et al.,
144 2002; Hammerle et al., 2007; Hiller et al., 2008; Goulden et al., 2012; Nadeau et al., 2013b; Stiperski &
145 Rotach, 2016), as it weakens flow distortion (Geissbühler et al., 2000; Oldroyd et al., 2016).

146 The Sapling flux tower is a 10-m triangular tower with one eddy-covariance system (IRGASON,
147 Campbell Scientific, USA) mounted at a height of 8.5 m, or ≈5 m above the canopy. As the tower is
148 located on a plateau, the instrument was leveled. Measurements from all eddy-covariance systems
149 were sampled at 10 Hz and logged separately on three CR3000 dataloggers (Campbell Scientific, USA).

150 The Juvenile and Sapling towers also featured measurements of net radiation and soil heat
151 flux. Net radiation was measured with 4-component radiometers (CNR4, Kipp and Zonen, The
152 Netherlands). At the Juvenile tower, two devices were mounted at 15 and 10 m above the surface and
153 parallel to 12° northeast-facing slope to follow the inclination of the eddy-covariance systems (Nadeau
154 et al., 2013a; Serrano-Ortiz et al., 2016). At the Sapling tower, one device was installed 7 m above the
155 ground and leveled.

156 The flux towers were also equipped with general meteorological measurements. Air
157 temperature and relative humidity were measured with standard probes (HC2S3 and HMP45C,

158 Campbell Scientific, USA). The Juvenile tower included a profile of four probes installed at heights of
159 3.29, 5.68, 10.77 and 14.96 m above the ground. The Sapling tower featured one probe at 2.10 m. Wind
160 speed and direction were measured using wind vanes (05103, RM Young, USA), namely, two of them
161 were installed at the Juvenile tower at heights of 8.53 and 14.63 m above ground, while one was
162 installed at 3 m above ground at the Sapling tower.

163 The Juvenile site also featured measurements of biomass temperature using a set of 39
164 thermistors (Omega Engineering, USA) placed in five trees around the flux tower (3 balsam firs, 1 white
165 spruce and 1 white birch). Three thermistors were installed in each tree trunk (one in the center of the
166 bole, one on the south side and one on the north side, both beneath the bark) at a height of 1.3 m. The
167 temperature of the top portion of each tree trunk was also monitored with thermistors placed on the
168 north and south sides beneath the bark at two-thirds of the tree height. 15 thermistors were installed
169 in tree branches: either on the top of the lowest branches or on the bottom of the top branches, on the
170 north and south sides of each monitored tree.

171 Total precipitation and complementary measurements of air temperature, relative humidity,
172 and atmospheric pressure were measured at a station located ≈ 4 km north of the study sites and
173 operated by the Québec government (MELCC, 2019). To obtain the most accurate snowfall
174 measurements, the site also had a Double-Fence Intercomparison Reference (DFIR, Pierre et al., 2019),
175 which is the reference to avoid solid precipitation under-catch (Yang, 2014). Data are available and
176 substituted to the regular station between November 1 and March 31 each year for the part of our
177 analysis that focuses on the Montmorency Forest watershed budget (see section 5.2). We did not use
178 DFIR data for the comparison between boreal sites (section 5.1), as the precipitation of the other sites
179 were not corrected for undercatch. Discrepancies in measurements with and without undercatch
180 corrections at Montmorency Forest are discussed in section 5.2.

181 The setup also includes discharge measurements, as illustrated in Figure 1a. Discharge were
182 obtained using v-notch weirs also operated by the Québec government (Station 51004 and 51007,
183 available at: https://www.cehq.gouv.qc.ca/hydrometrie/historique_donnees/). Daily mean runoffs
184 were used in this study.

185

186 *2.3. Data processing*

187 Eddy-covariance raw 10-Hz measurements were processed using EddyPro[®], version 6.0 (LI-
188 COR Biosciences, USA). The procedure included linear detrending, correction of low-pass (Moncrieff
189 et al., 1997) and high-pass (Moncrieff et al., 2004) filtering effects, covariance maximization, density
190 fluctuations compensation with the Webb correction (Webb et al., 1980). Coordinate rotation of wind
191 speed was performed using a sector-wise planar fit (Wilczak et al., 2001), since this procedure is
192 recommended for eddy-covariance measurements on slopes (Ono et al., 2008; Oldroyd et al., 2016).
193 Spikes, amplitude resolution artifacts, unrealistic drop-outs, outliers and discontinuities, as well as
194 other artifacts were detected and removed using the statistical tests of Vickers & Mahrt (1997).

195 Turbulent fluxes were computed using a 30-min averaging period. Errors associated with fluxes were
196 quantified using the random uncertainty method of Finkelstein & Sims (2001).

197 Data runs during rainfall events were filtered out, because rain can obstruct the path of the
198 open gas analyzer light signal. Periods when winds were blowing from a 90° sector centered on the
199 back of the devices were also removed, as these conditions imply that the flow of air is distorted by the
200 tower structure. Poor data quality was assessed and removed using the 0-1-2 criteria of Mauder &
201 Foken (2011). Periods when turbulent fluxes largely violated the energy budget (*i.e.*, $H + \lambda E > 5R_n$) were
202 discarded. Filtering was completed by a meticulous visual inspection to detect and remove periods of
203 clear malfunction. This rigorous filtering procedure removed $\approx 35\%$ and $\approx 50\%$ of data segments for H
204 and λE , respectively, for both sites between 2016 and 2018 inclusively.

205 For the Juvenile site, time series of fluxes from both eddy-covariance setup were combined
206 using wind direction. To further complete these time series, the Juvenile and Sapling fluxes were gap-
207 filled using marginal distribution sampling (MDS) as described in Reichstein et al. (2005) (see their
208 Appendix A and Figure A1), as recommended by Moffat et al. (2007). This procedure left only $\approx 5\%$ and
209 $\approx 20\%$ of missing data for H and λE , respectively. Remaining gaps were filled with monthly linear
210 regression with zero-set origin between fluxes and net radiation.

211 As was the case for eddy-covariance data, all complementary meteorological and biomass
212 temperature measurements were subjected to a rigorous filtering procedure that began with a careful
213 visual inspection to detect clear periods of malfunction. Some meteorological variables received
214 specific filtering procedures. Shortwave downwelling radiation was capped by maximum theoretical
215 values calculated following Whiteman & Allwine (1986). For every temperature-humidity sensor,
216 humidity values were capped using temperature-dependent maximum humidity.

217 For every variable, gap-filling was performed by merging time series from different devices
218 with monthly linear regressions using a clear step-by-step procedure: (i) a variable is filled with other
219 on-site devices by order of proximity; (ii) variable are next filled with the other site similar devices;
220 and (iii) the few remaining gaps are completed with data from the nearby governmental station.

221 Soil heat fluxes were measured with soil heat flux plates, but energy storage above the plates
222 (ΔQ_G [W m^{-2}]) were also calculated and included in G . They were obtained from the standard
223 calorimetric method (Ochsner et al., 2007):

224

$$225 \quad \Delta Q_G = c_p \frac{\Delta T_s}{\Delta t} \Delta z \quad (3)$$

226

227 where ΔT_s [K] is the difference in soil temperature T_s between two time steps of length Δt [s]; Δz [m] is
228 the soil layer thickness between the plates and the surface; and c_p [$\text{J m}^{-3} \text{K}^{-1}$] is the specific heat of the
229 soil, taken as:

230

231
$$c_p = c_{p,dry} + c_{p,water} \theta \quad (4)$$

232

233 where $c_{p,dry}$ and $c_{p,water}$ are values taken from the literature for a sandy loam and for water (1.28×10^6
 234 and $4.184 \times 10^6 \text{ J m}^{-3} \text{ K}^{-1}$, respectively; Van Wijk, 1963) and $\theta [\text{m}^3 \text{ m}^{-3}]$ is the volumetric water content
 235 of the soil.

236 Soil heat flux plates were subject to very frequent malfunctions. Fortunately, ΔQ_G
 237 measurements were almost continuous once on-site time series were merged, and correlation
 238 between soil heat flux plates measurements and ΔQ_G were high (R^2 between 0.7 and 0.9). Missing G
 239 values were obtained using a monthly linear regression with ΔQ_G .

240 To account for the measurement height of the eddy-covariance systems, storage fluxes of
 241 sensible heat and latent heat (ΔQ_H and $\Delta Q_{\lambda E}$) were also evaluated at each station using the method of
 242 Aubinet et al. (2001):

243

244
$$\Delta Q_H = \sum_{i=1}^4 c_{p,i} \rho_i \frac{\Delta T_i}{\Delta t} \Delta z_i \quad (5)$$

245

246
$$\Delta Q_{\lambda E} = \sum_{i=1}^4 L_{v,i} \rho_i \frac{\Delta q_i}{\Delta t} \Delta z_i \quad (6)$$

247

248 where subscript i applies to the four (one) measurement height for each variable of the Juvenile
 249 (Sapling) station; $\Delta T_{a,i} [\text{K}]$ and $\Delta q_i [\text{kg kg}^{-1}]$ are the differences in T_a or q at height i between two time
 250 steps of length Δt [s]; and Δz_i [m] is the air layer thickness associated with each measurement probe.
 251 For the Juvenile station, Δz_i is 4.49 m, 3.74 m, 4.64 m and 1.50 m from bottom to top probe, respectively,
 252 while Δz is the measurement height (8.5 m) for the Sapling station.

253 Biomass heat storage (ΔQ_B) was computed for specific portion (upper and lower trunk,
 254 branches, needles or leaves) of each monitored tree using vegetation temperature measurements and
 255 the following general formula (Oliphant et al., 2004):

256

257
$$\Delta Q_{veg} = m_{veg} c_{p,veg} \frac{\Delta T_{veg}}{\Delta t} \quad (7)$$

258

259 where $\Delta Q_{veg} [\text{W}]$ is a heat storage within a specific tree portion; $m_{veg} [\text{kg}]$ is its mass [kg]; $c_{p,veg}$ is its heat
 260 capacity [$\text{J kg}^{-1} \text{ K}^{-1}$]; and ΔT_{veg} is the temperature variation during a time step of length Δt .

261 Specific properties of the trees were obtained from USDA (2007). Tree trunk portions were
 262 approximated as cylinders, and bulk temperature variations of the upper and lower trunks as a whole
 263 were calculated using the method outlined in Garai et al. (2010). Branch and needle temperatures were

264 taken as the average of branch thermistors. Branch mass was calculated using surveyed branch density
265 with height and assuming that branch length decreases linearly from the bottom branches to the top
266 of the tree. Needle mass was calculated using the empirical functions of Ter-Mikaelian & Korzukhin
267 (1997). ΔQ_B was then taken as the sum of ΔQ_{veg} values from trunk, branch and needle for each tree
268 species (the three balsam firs were averaged), and multiplied by species-specific stem densities
269 surveyed around the flux tower (balsam fir: 0.26 m^{-2} ; white spruce: 0.01 m^{-2} ; white birch: 0.003 m^{-2}).
270 Missing ΔQ_B values were filled with monthly linear regression with zero-set origin between heat
271 storage and net radiation.

272

273 3. Comparison Sites

274 The energy budgets of the Montmorency Forest sites were compared to those of 15 sites
275 located in the boreal forest that are described in Table 1. Data from European (BS1858, SP1907,
276 SP1962) and United States (BS1945) sites were obtained from the Fluxnet 2015 dataset (available at:
277 <https://fluxnet.fluxdata.org>), while data from Canadian sites were part of the FLUXNET Canada
278 Research Network Canadian Carbon Program Data Collection, 1993-2014 (FLUXNET-Canada, 2016).
279 Note that the Juvenile and Sapling sites are also featured in Table 1 as sites BF1993 and BF2003,
280 respectively.

281 The sites used for comparisons are spread all across the circumpolar boreal biome and include
282 most of the usual trees found in these regions at different stages of maturity. Annual averages of
283 temperature are relatively constant throughout the sites, with variations between -2.0°C in Alaska
284 (BS1945) and 3.9°C in Russia (BS1858). Climatological averages of annual cumulative precipitation
285 vary greatly across sites, from the very dry Alaskan site (275 mm y^{-1}) to the humid sites of eastern
286 Canada (MW1980 at 831 mm y^{-1} ; BS1912, BS1975 and BS2000 at 961 mm y^{-1}), culminating at the
287 main study sites in the Montmorency Forest receiving an average of 1583 mm y^{-1} .

288 Table 1 also presents the main references for each study site, in which instrumental setups are
289 described. All sites featured standard eddy-covariance systems installed following diligent procedures.
290 Data from the Fluxnet 2015 dataset was processed following methods outlined at
291 <https://fluxnet.fluxdata.org/data/fluxnet2015-dataset/data-processing/>: every variable is rigorously
292 quality-checked (Pastorello et al., 2014), meteorological variables are gap-filled using ERA-Interim
293 reanalysis (Vuichard & Papale, 2015), while turbulent fluxes are gap-filled with the standard MDS
294 procedure (Reichstein et al., 2005). FLUXNET-Canada (2016) dataset was processed following similar
295 procedures described in Papale & Valentini (2003); Reichstein et al. (2005); Papale et al. (2006);
296 Moffat et al. (2007).

297 In this study, we first present the fluxes that were uncorrected for energy balance closure (see
298 section 5.1.1). To account for missing flux values at each site, we linearly scaled monthly sums of
299 energy; multiplying the latter by the ratio of total number of periods in a given month over periods of

300 available data in the same month. Note that this procedure was also applied for annual sums of E and
301 P .

302 This study also presents annual sums of E as components of the water budget at each site.
303 However, every site experiences non-closure of the energy budget on a yearly basis (see section 5.1.1).
304 Energy budget imbalance is a common problem with studies using eddy-covariance fluxes (*e.g.*,
305 Baldocchi et al., 1997; Barr et al., 2001; 2006; Foken et al., 2010; Isabelle et al., 2018b), where the
306 technique measures smaller turbulent fluxes ($H + \lambda E$) than the available energy ($R_n - G - \Delta Q$). Probable
307 causes behind this anomaly are well-described by Foken (2008), Leuning et al. (2012), and Stoy et al.
308 (2013), among others. The consequence of this imbalance is that uncertainties are associated with E
309 measurements, which are probably underestimated at all sites. For this reason, annual sums of E have
310 to be corrected in water balance studies (Wohlfahrt et al., 2010).

311 In the present study, closure fraction (CF) was evaluated as the annual sums of turbulent fluxes
312 ($H + \lambda E$) divided by the annual sums of available energy ($R_n - G - \Delta Q$). However, precise and accurate
313 measurements of G and ΔQ were not available at all sites: to be consistent for the sake of site
314 comparison, we computed annual sums of available energy using only R_n . The relevance of this
315 assumption is discussed in section 5.1.1. Annual E was then obtained by dividing measured annual E
316 by annual CF , a method that preserves the Bowen ratio, *i.e.* the proportion of H to λE (Blanken et al.,
317 1997; Twine et al., 2000; Wohlfahrt et al., 2010). This energy imbalance correction method was
318 successfully applied in a hydrological study of the BOREAS region, in the Western Great Plains of
319 Canada (Barr et al., 2012), and deemed appropriate to account for the underestimation of E in eddy-
320 covariance measurements (Mauder et al., 2018).

321

322 Table 1: Description of the study sites. Site IDs are generated with main tree species at the site (first two letters) and approximate year of the last on-site disturbance, when vegetation started
323 to grow back (last four numbers). LAI is the leaf area index at the start of the site study period, while GS is the average growing season length in days [d], calculated using the method of
324 Bergeron et al. (2007). T_a and P are climatological averages of T_a and P on an annual basis. Age of tree stand is at the start of the site study period, described in the “Study years” column.

Site ID	Location	Coordinates	Altitude [m AMSL]	Vegetation (Age [y])	LAI [m ² m ⁻²]	Study years	GS [d]	T_a [°C]	P [mm]	Reference
AS1928	Saskatchewan, Canada	53.63°N; 106.20°W	601	Aspen (70)	3.8	1997-2000; 2002-2010	227	0.4	467	Blanken et al. (1998)
BF1993	Québec, Canada	47.29°N; 71.17°W	855	Balsam Fir (25)	3.4	2016-2018	198	0.5	1583	Isabelle et al. (2018)
BF2003	Québec, Canada	47.29°N; 71.15°W	805	Balsam Fir (10)	2.9	2016-2018	199	0.5	1583	This study
BS1858	Fyodorovskoye, Russia	56.46°N; 32.92°E	265	Black Spruce (140)	3.5	1999-2012	268	3.9	711	Kurbatova et al. (2008)
BS1880	Saskatchewan, Canada	53.99°N; 105.11°W	629	Black Spruce (120)	5.6	2001-2010	216	0.4	467	Jarvis et al. (1997)
BS1912	Québec, Canada	49.69°N; 74.34°W	382	Black Spruce (95)	4.0	2005-2009	221	0.0	961	Bergeron et al. (2007)
BS1945	Alaska, USA	65.12°N; 147.49°W	210	Black Spruce (65)	0.7	2011-2012; 2014	173	-2.0	275	Ikawa et al. (2015)
BS1975	Québec, Canada	49.76°N; 74.57°W	385	Black Spruce (35)	3.5	2008-2010	233	0.0	961	Payeur-Poirier et al. (2012)
BS2000	Québec, Canada	49.27°N; 74.04°W	415	Black Spruce (5)	1.6	2005-2010	225	0.0	961	Giasson et al. (2006)
JP1915	Saskatchewan, Canada	53.92°N; 104.69°W	579	Jack Pine (90)	2.0	2004-2009	215	0.4	467	Baldocchi et al. (1997)
JP1975	Saskatchewan, Canada	53.88°N; 104.65°W	534	Jack Pine (30)	3.1	2005-2006	205	0.4	467	Mkhabela et al. (2009)
JP2002	Saskatchewan, Canada	53.94°N; 104.65°W	520	Jack Pine (5)	0.2	2005-2007	207	0.4	467	Mkhabela et al. (2009)
MW1930	Ontario, Canada	48.22°N; 82.16°W	340	Mixed Forest (75)	4.1	2006-2013	240	1.3	831	McCaughey et al. (2006)
SP1907	Sodankylä, Finland	67.36°N; 26.64°E	179	Scots Pine (110)	3.8	2003-2004	208	-0.4	527	Thum et al. (2007)
SP1962	Hyytiälä, Finland	61.85°N; 24.29°E	181	Scots Pine (35)	7.9	1997-2010	276	2.9	709	Suni et al. (2003)

326 **4. Potential evapotranspiration calculation**

327 This study focused on the effect of high precipitation on E , as it is viewed as a good proxy for
 328 water availability that can constrain land-atmosphere exchanges of water. However, to put
 329 comparison sites in perspective, it is also important to quantify site-specific values of the energy
 330 available for E and the potential water vapor content of the atmosphere. These concepts are well-
 331 described using potential evapotranspiration (E_p).

332 To evaluate E_p , we used the formula developed by Penman (1948). This equation was
 333 originally devised to quantify evaporation from an open-water surface, but it can also apply to
 334 saturated land surfaces. It combines energy-balance and mass-transfer approaches to evaluate E_p from
 335 available energy (R_n) and from atmospheric vapour deficit, which determines drying power of the air
 336 (ϕ). The equation goes as follows:

337

$$338 \quad E_p = \frac{1}{\lambda} \left[\frac{\Delta_e}{(\Delta_e + \gamma)} R_n + \frac{\gamma}{(\Delta_e + \gamma)} \phi \right] \quad (8)$$

339

340 where E_p [$\text{kg m}^{-2} \text{s}^{-1}$] is the potential water vapor flux; λ [J kg^{-1}], the latent heat of vaporisation of water;
 341 Δ_e [Pa K^{-1}], the slope of saturation vapour pressure versus temperature curve; γ [Pa K^{-1}], the
 342 psychrometric constant; R_n [W m^{-2}], the net radiation; and ϕ [W m^{-2}], the drying power of the air
 343 defined by Katul & Parlange (1992) as:

344

$$345 \quad \phi = \frac{c_p \kappa^2 \rho U D}{\gamma \ln\left(\frac{z_v - d_0}{z_{0v}}\right) \ln\left(\frac{z_m - d_0}{z_{0m}}\right)} \quad (9)$$

346

347 where c_p [$\text{J kg}^{-1} \text{K}^{-1}$] is the specific heat of the humid air; κ , the von Kármán constant ($= 0.4$); ρ [kg m^{-3}],
 348 the humid air density; U [m s^{-1}], the mean wind velocity measured at height z_m [m]; D [Pa], the vapor
 349 pressure deficit measured at height z_v [m]; γ [Pa K^{-1}], the psychrometric constant; z_{0m} and z_{0v} [m], the
 350 roughness lengths for momentum and humidity, respectively; d_0 [m], the zero-plane displacement
 351 height. d_0 , z_{0m} , and z_{0v} are estimated with the site-specific mean vegetation height (h_v) (see Table 1) as
 352 $(2/3)h_v$, $0.1h_v$, and $0.01h_v$, respectively (Brutsaert, 1982; 2005).

353 Note that this evaluation of E_p is a theoretical upper bound: in reality, soil heat fluxes (G), and
 354 heat storage in biomass and air below measurement devices (ΔQ) should be subtracted from R_n to
 355 obtain available energy. Unfortunately, as was previously mentioned, these energy budget terms were
 356 not available at every comparison sites. To preserve consistency between measurement sites and be

357 consistent with E adjustments for closure fraction, we decided to compute E_p using only R_n , while
358 noting that this probably results in an overestimation of E_p .

359

360 **5. Results and Discussion**

361 *5.1. Comparison between boreal forest sites*

362 *5.1.1. Energy budget*

363 Figure 2 presents annual cycles of monthly-averaged energy budget terms for each study site,
364 for daytime periods only ($R_n > 0$), as it is when the majority of fluxes occur. Each plot includes one
365 curve for each term per study year to outline interannual variability. Note that H and λE are here shown
366 without energy imbalance correction. All study sites are characterized by classical net radiation curves
367 culminating during (Northern Hemisphere) summer months, with obviously a very slight tendency
368 towards higher values at southernmost latitudes (*e.g.*, SP1907 at 67.36°N has maximum $R_n \approx 400 \text{ W m}^{-2}$
369 vs. SP1962 at 61.85°N has maximum $R_n \approx 455 \text{ W m}^{-2}$). All sites share similar annual trends: spring
370 increases in R_n are counterbalanced by increasing H at first, but λE fluxes eventually rise around June
371 when the growing season (and transpiration) blooms. The main difference between sites lies in the
372 magnitude of summer λE peaks and the proportion of R_n they account for.

373 Two behaviours are exhibited in Figure 2: pine stands (JP1915, JP1975, JP2002, SP1907, and
374 SP1962) and some black spruce stands (BS1858, BS1880, BS1912, and BS1945) see λE increasing in
375 the summer without usually exceeding H , while other sites show a clear dominance of λE in the energy
376 budget at the summer onset of transpiration. These discrepancies can stem from three plausible
377 sources: (i) tree species; (ii) age of the tree stand; and (iii) meteorological conditions governing direct
378 water and energy availability. The first two sources represent land surface conditions including soil
379 type and moisture conditions.

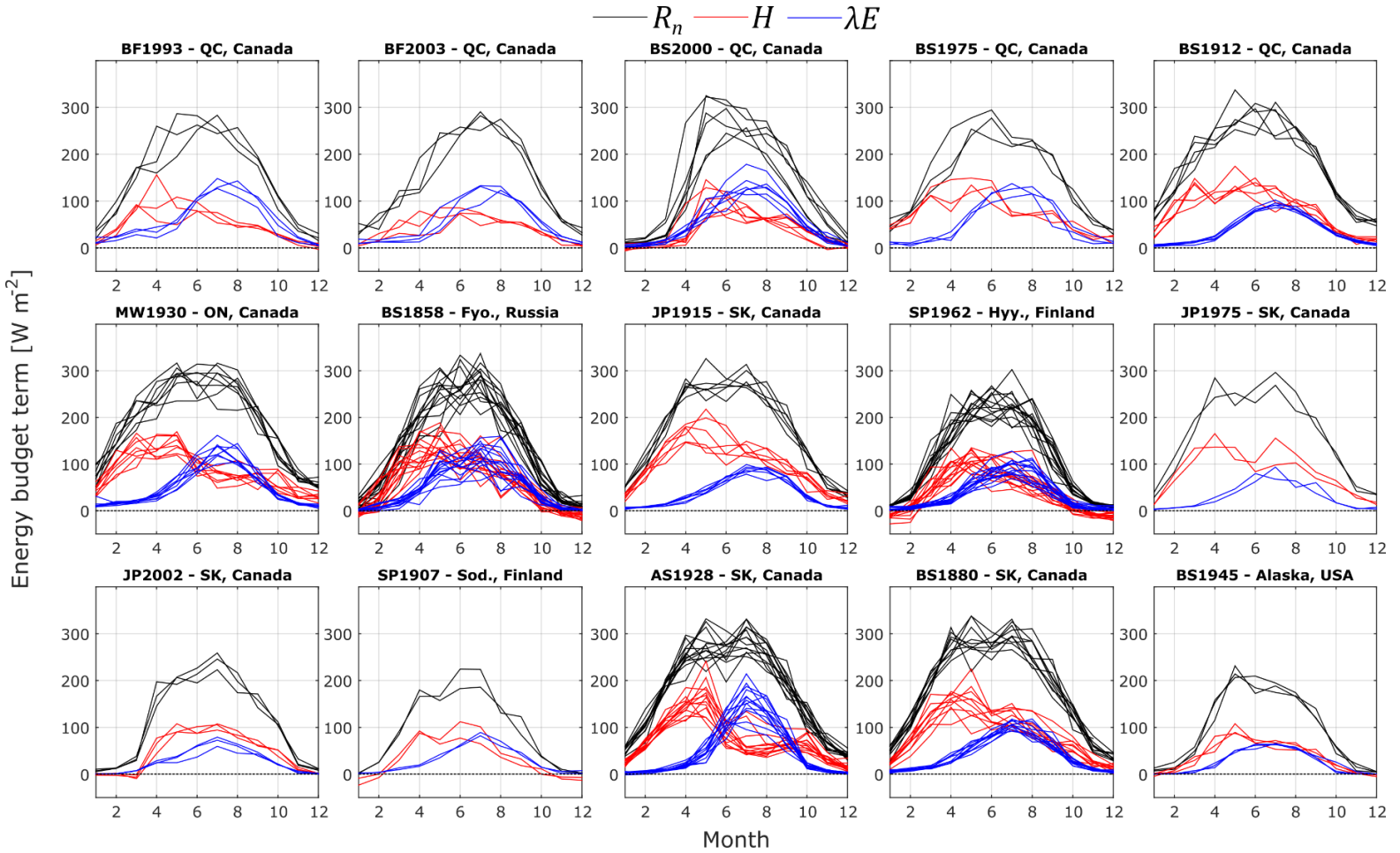
380 Differences in energy budget across tree species are clear: stands including a large proportion
381 of deciduous species (AS1928 and MW1930) exhibit a more pronounced summer peak in λE , the
382 upward inflection point coinciding with leaf emergence. Balsam firs and black spruces usually thrive
383 in wet environments and generate substantial λE given adequate water availability (McCaughey, 1978;
384 Nijssen & Lettenmeier, 2002). On the contrary, pine stands grow in sandy well-drained soil and
385 consequently produce lower λE fluxes (Nijssen & Lettenmeier, 2002; Mkhabela et al., 2009).

386 Pine stands appear to generate similar λE fluxes at different stages of maturity, as seen by
387 comparing SP1907 with SP1962 or JP1915 with JP1975 and JP2002. The same can be said of balsam
388 firs (BF1993 and BF2003), but black spruce stands from eastern Canada feature some differences.
389 Indeed, the mature black spruces of BS1912 generate a notably lower summer peak of λE compared to

390 the juvenile stands of BS1975 or the saplings of BS2000. This behaviour is more thoroughly inspected
391 in the next section.

392 All surveyed sites are subject to non-closure of the annual energy budget. Closure fraction (CF)
393 varies between 0.50 and 0.99, while the interannual site averages vary between 0.69 (BS1945) and
394 0.90 (JP1915). Wherever the inclusion of other important energy budget terms such as G and/or ΔQ
395 was possible, yearly values of CF did not improve much, with variations between -0.01 and 0.08 and
396 an average variation of 0.01 . For this reason, it seems that adjusting annual E values for energy budget
397 closure using only R_n as available energy is a reasonable decision. It creates minimal uncertainties in
398 yearly CF , and hence yearly E , and it is the most coherent procedure to apply to all sites.

399



400

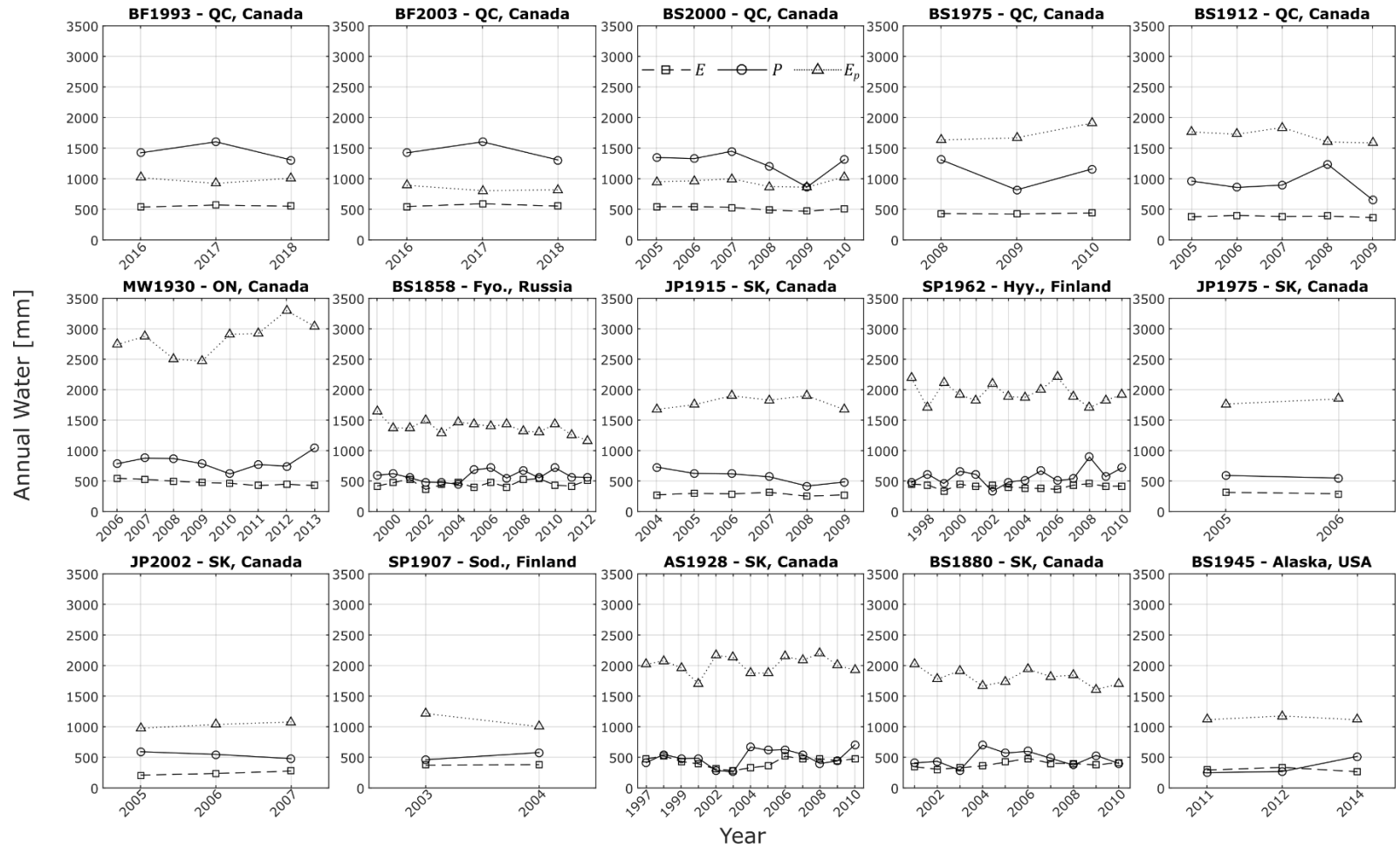
401 Figure 2: Annual cycles of monthly averaged net radiation (R_n , black lines) and sensible and latent heat fluxes (H and λE , uncorrected for energy imbalance, red and blue lines, respectively) for
 402 all study sites, including only daytime observations, defined as when $R_n > 0$). Each graph features one curve per study year for each variable. Sites are ordered by annual cumulative
 403 precipitation, from the site receiving most precipitation (BF1993) to the site receiving less (BS1945).

404 5.1.2. *Evapotranspiration and precipitation*

405 Yearly-scale variations of E and P as well as site-dependent evaporative demands (E_p) are
406 outlined in Figure 3 and described in details in Table 2. All values of E are corrected for energy
407 imbalance. These results bring forward the trends outlined in the previous section: sites with higher
408 summer peaks of λE (AS1928, BF1993, BF2003, BS1975, BS2000, and MW1930) evidently are the sites
409 enduring the strongest yearly E rates. The latter fluctuate amongst sites, from 194 mm y^{-1} for JP2002
410 to 446 mm y^{-1} at the Montmorency Forest juvenile balsam fir stand (BF1993).

411 Precipitation rates, as a proxy of water availability, appear very influential in the distribution
412 of E rates, as can be seen in Table 2. Montmorency Forest sites (BF1993 and BF2003) clearly stand out
413 as the sites receiving the most precipitation by a large margin, and consequently returning the greatest
414 amount of water back to the atmosphere. In general, ranking sites by E rates or by P rates yields similar
415 results, aside from some notable outliers. For example, AS1928 and BS1880 evaporate 422 and 383
416 mm y^{-1} ; good for 7th and 9th rank by E , respectively, despite receiving the second and third lowest yearly
417 precipitation. These sites are however characterized by strong energy inputs, as demonstrated by their
418 very high E_p rates (2014 and 1806 mm y^{-1} , good for 2nd and 5th rank by E_p , respectively). Note that these
419 findings stand with or without energy imbalance corrections. Such similarities between ranks are not
420 visible when ranking sites by E and E_p , which seems to imply that boreal forest E strongly depends on
421 water availability.

422 However, there is an intricate relationship between E , water availability (P) and evaporative
423 demand (E_p). Figure 4 summarizes that relationship for each study site, that is: yearly-summed
424 evaporative index (E/P) as a function of yearly-summed aridity index (E_p/P). The figure emulates the
425 classical Budyko framework (Budyko, 1958, 1974), but note that this framework usually applies to
426 climatologic rather than yearly averages (Gentine et al., 2012). The Montmorency Forest sites again
427 stand out (blue circles and triangles): the sites have very low values of evaporative index and the
428 lowest values of aridity index. Even if they generate the largest yearly evaporative rates, the important
429 precipitation still outweighs evaporative losses by a lot. Recurring precipitation also decreases sun
430 exposure and increase air humidity, which limits the potential to evaporate, indicating that water
431 availability is rarely an issue.



432

433 Figure 3: Interannual variations of annual cumulative precipitation P (full lines with circles), potential evapotranspiration E_p (dotted lines with triangles) and evapotranspiration E (dashed
 434 lines with squares) for each study site. Cumulatives are adjusted to account for missing values (see section 3). Sites are placed by annual precipitation rate ranking, from the site receiving
 435 most precipitation (BF1993) to the site receiving less precipitation (BS1945).

436 Table 2: Interannual averages \pm standard deviations of E , E^* (uncorrected for energy imbalance), P and E_p for each study site,
 437 for the number of years in the second column. P_{clim} is the climatological average of precipitation (from Table 1). Sites are ordered
 438 by annual precipitation rate, from the site receiving the most precipitation (BF1993) to the site receiving the less precipitation
 439 (BS1945).

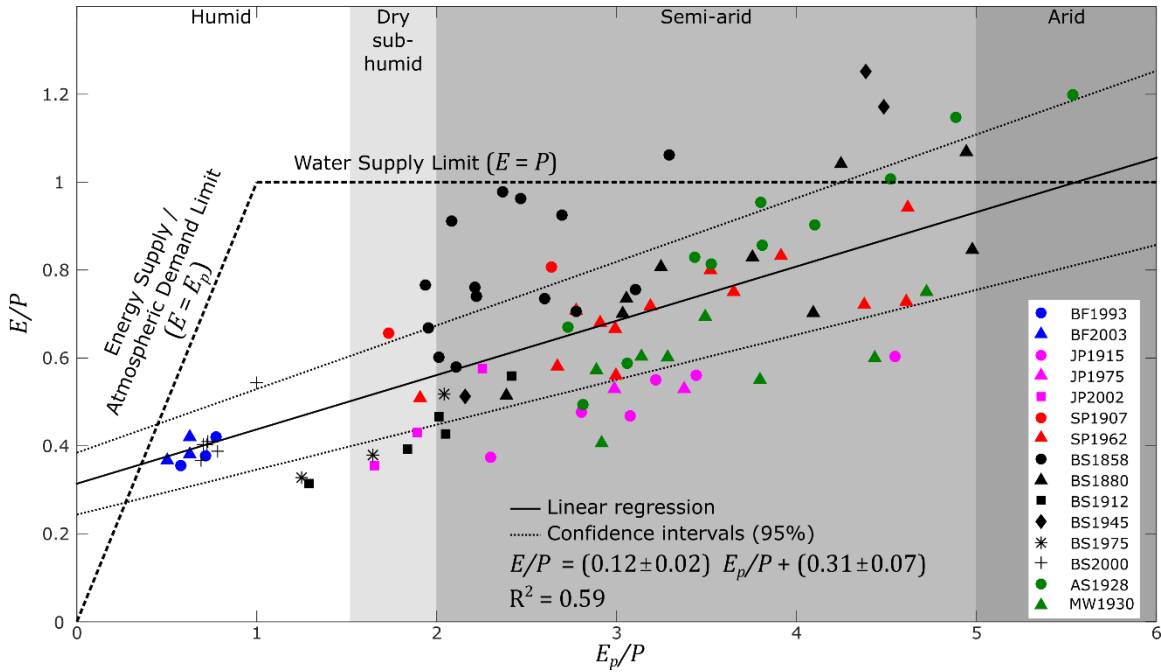
440

Site ID	# of years	P_{clim} [mm y ⁻¹]	E [mm y ⁻¹]	E^* [mm y ⁻¹]	P [mm y ⁻¹]	E_p [mm y ⁻¹]
BF1993	3	1583	552 \pm 17	446 \pm 33	1444 \pm 149	983 \pm 52
BF2003	3	1583	562 \pm 25	403 \pm 55	1444 \pm 149	839 \pm 47
BS2000	6	961	514 \pm 31	425 \pm 40	1251 \pm 205	946 \pm 68
BS1975	3	961	431 \pm 9	382 \pm 9	1096 \pm 252	1737 \pm 151
BS1912	5	961	383 \pm 12	286 \pm 13	922 \pm 211	1703 \pm 108
MW1930	8	831	476 \pm 45	380 \pm 44	811 \pm 123	2845 \pm 274
BS1858	14	711	457 \pm 55	353 \pm 51	585 \pm 87	1384 \pm 117
JP1915	6	467	283 \pm 22	253 \pm 15	574 \pm 110	1788 \pm 105
SP1962	14	709	411 \pm 35	300 \pm 48	574 \pm 137	1940 \pm 163
JP1975	2	467	303 \pm 16	218 \pm 1	569 \pm 31	1806 \pm 59
JP2002	3	467	240 \pm 33	194 \pm 25	539 \pm 57	1030 \pm 51
SP1907	2	527	375 \pm 5	276 \pm 11	536 \pm 52	1012 \pm 102
AS1928	13	467	422 \pm 79	370 \pm 59	498 \pm 138	2014 \pm 142
BS1880	10	467	383 \pm 52	311 \pm 22	479 \pm 116	1806 \pm 126
BS1945	3	275	297 \pm 36	202 \pm 8	344 \pm 149	1135 \pm 36

441

442 Figure 4 displays an obvious trend amongst study sites: increasing the aridity index usually
 443 results in larger evaporative indexes, *i.e.*, the more arid the environment, the greater the proportion of
 444 P that is returned to the atmosphere. Note that the featured linear regression is statistically significant
 445 (p -value $<$ 0.05). If we rearrange the linear regression equation, we obtain that $E = 0.12E_p + 0.31P$. This
 446 equation cannot be used single-handedly as a model for predicting annual E , but it outlines nicely the
 447 contribution from evaporative demand (E_p) and water availability (P) to E in boreal forests of the
 448 world. It also corroborates previous results that seem to point out to a slightly larger impact of water
 449 availability, or precipitation, to annual E . These trends are similarly visible when using E without
 450 energy imbalance corrections (not shown). Figure 4 also depicts the large interannual variability of
 451 most sites as well as uncertainty issues regarding the estimation of E and E_p , *e.g.*, E/P are above 1 in
 452 some situations.

453



454

455 Figure 4: Evaporative index (evapotranspiration divided by precipitation E/P) vs. aridity index (potential evapotranspiration
 456 divided by precipitation E_p/P) for each study site. Each point represent one study year annual sums of E , P and E_p . Dashed lines
 457 show the demand limit (maximum possible E based on energy supply / atmospheric demand) and water supply limit
 458 (maximum E based on available water). Solid line is a least-squared linear regression with coefficients and R^2 introduced at the
 459 bottom of the graph, while dotted lines are the 95% confidence intervals lines corresponding to errors in linear regression
 460 coefficients.

461 We used multiple linear regressions to isolate the primary controls on annual
 462 evapotranspiration. The latter, for all sites and measurement years, was taken as the response
 463 variable, with predictors being annual precipitation (P [mm]), annual potential evapotranspiration (E_p
 464 [mm]), latitude (φ [°]), altitude (z [m]), and stand age (A [y]). The model took the following form:

465

$$466 \quad E = 170 \text{ mm} + 0.21 \frac{\text{mm}}{\text{mm}} P + 0.02 \frac{\text{mm}}{\text{mm}} E_p + 0.73 \frac{\text{mm}}{\text{°}} \varphi - 0.04 \frac{\text{mm}}{\text{m}} z + 0.49 \frac{\text{mm}}{\text{y}} A \quad (10)$$

467

468 and had an R^2 value of 0.40 while being statistically significant (p-value < 0.05). Interestingly, only P
 469 and A were significant contributors to the model (p-value < 0.05). These results highlight the high
 470 importance of annual precipitation on annual evapotranspiration. In addition, they identify stand age
 471 as an important predictor for annual E . Observations point towards minimal influences of latitude,
 472 altitude, and (more surprisingly) potential evapotranspiration. Latitude and annual precipitation are
 473 linked ($R^2 = 0.37$, p-value < 0.05) but not altitude and annual precipitation, primarily because all

474 Saskatchewan sites (AS1928, BS1880, JP1915, JP1975, and JP2002) have relatively high altitude (~565
 475 m AMSL) and low precipitation.

476 The analysis was repeated species by species, whenever the number of data points allowed
 477 for it (*i.e.* not for balsam firs only and jack pines only; grouping aspens with mixed woods as
 478 “deciduous”; and grouping jack pines with scots pines as “pines”). Table 3 presents the coefficient of
 479 determination for each of these subset models, along with the associated p-values.

480
 481 Table 3: Summary of multiple linear regressions results. Coefficient of determination R^2 are shown for models found for each
 482 groups of study sites. p-values indicate the significance level of each variables in the model: values in bold are significant at the
 483 5% confidence level. Dashes indicate that the intercept value of the particular model was zero. Whenever a model has no
 484 significant contributing variable, the one with lowest p-value is in italics.

Groups	R^2	Intercept	p-value				
			P	E_p	φ	z	A
All	0.40	0.41	0.00	0.20	0.78	0.49	0.01
Deciduous	0.24	-	<i>0.18</i>	<i>0.77</i>	0.27	0.71	0.47
Conifers	0.53	0.72	0.00	0.43	0.29	0.21	0.00
Black Spruce	0.55	0.00	0.14	0.00	0.06	0.82	0.00
Scots Pine	0.32	-	0.54	<i>0.37</i>	0.96	0.75	0.52
Pines	0.85	0.55	<i>0.12</i>	0.34	0.80	0.22	0.58

486
 487 These results show quite well that annual precipitation is commonly a driving factor in annual
 488 evapotranspiration, except maybe for Scots pines, which is mostly the SP1962 site. Stand age is the
 489 second most important variable: particularly for black spruces. Potential evapotranspiration is
 490 particularly influential for black spruces, and mildly for Scots pines and pines in general. Latitude and
 491 altitude again do not appear to be of influence.

492 As was described in section 4, E_p combines the effects of available energy, air humidity and
 493 atmospheric water vapor holding capacity to obtain maximum possible E . In Table 4, we quantify these
 494 effects by computing linear regressions between monthly summed E and monthly summed R_n or
 495 monthly averaged D (vapor pressure deficit) for all study site. Results show that R_n and D are important
 496 drivers of E : R_n explains between 60% and 89% of E variance, while D explains between 62% and 94%
 497 of E variance. All described linear regressions and correlations are statistically significant (p-value <
 498 0.05), and these results are also observed with E uncorrected for energy imbalance (not shown).
 499 Similar results were obtained by Brümmer et al. (2012) for various Canadian sites (including AS1928,
 500 BS1880, BS1912, JP1915, and MW1930).

501 For most sites, correlation between E and D is close to or higher than correlation between E
 502 and R_n . BS1858 is the outlier, with R^2 values at 0.82 and 0.62 for linear regressions between E and R_n
 503 or D , respectively. Conifer-dominated sites in Saskatchewan exhibit smaller $E - D$ and $E - R_n$ slopes

504 than other sites, highlighting their tendency to limit E under low water availability conditions, even in
 505 times of high evaporative demand.

506

507 Table 4: Linear regression parameters (slope and intercept, with 95% confidence intervals) and coefficient of determination
 508 (R^2) between monthly summed E and: (i) monthly summed net radiation R_n ; and (ii) monthly average 24-h vapour pressure
 509 deficit D .

Site ID	E vs. R_n			E vs. D		
	Slope [mm/(M) m ⁻²]	Intercept [mm month ⁻¹]	R^2	Slope [mm/Pa]	Intercept [mm month ⁻¹]	R^2
AS1928	0.22 ± 0.03	0.30 ± 6.17	0.61	0.12 ± 0.01	-8.53 ± 6.37	0.66
BF1993	0.19 ± 0.05	13.46 ± 11.99	0.60	0.18 ± 0.04	8.32 ± 10.06	0.74
BF2003	0.25 ± 0.05	6.04 ± 9.85	0.77	0.19 ± 0.04	8.88 ± 10.57	0.72
BS1858	0.22 ± 0.02	1.16 ± 3.68	0.82	0.12 ± 0.01	4.58 ± 5.41	0.62
BS1880	0.15 ± 0.02	2.61 ± 4.41	0.72	0.09 ± 0.01	-0.03 ± 3.46	0.83
BS1912	0.16 ± 0.03	-0.16 ± 7.30	0.67	0.10 ± 0.01	2.50 ± 4.18	0.86
BS1945	0.15 ± 0.02	5.04 ± 3.98	0.89	0.10 ± 0.01	-5.32 ± 5.39	0.87
BS1975	0.21 ± 0.04	-1.17 ± 9.61	0.74	0.13 ± 0.02	1.31 ± 7.39	0.82
BS2000	0.22 ± 0.02	8.43 ± 5.25	0.84	0.13 ± 0.01	0.40 ± 6.11	0.83
JP1915	0.12 ± 0.02	4.17 ± 4.48	0.66	0.07 ± 0.01	-0.51 ± 3.26	0.84
JP1975	0.15 ± 0.04	1.21 ± 8.28	0.75	0.08 ± 0.02	-2.90 ± 7.93	0.80
JP2002	0.13 ± 0.02	5.49 ± 3.19	0.87	0.06 ± 0.01	-1.64 ± 2.62	0.94
MW1930	0.20 ± 0.03	-0.90 ± 6.99	0.68	0.11 ± 0.01	0.29 ± 6.28	0.72
SP1907	0.18 ± 0.04	6.94 ± 8.74	0.77	0.13 ± 0.03	3.86 ± 8.00	0.82
SP1962	0.20 ± 0.01	5.09 ± 3.06	0.82	0.12 ± 0.01	1.08 ± 3.46	0.80

510

511 We must remind readers that E_p values calculated in this study are considered to be upper
 512 bounds, since the available energy used in the Penman formulation includes only R_n without G and ΔQ .
 513 However, as was seen in section 5.1.1, differences in available energy following the inclusion of G
 514 and/or ΔQ are fairly inconsequential on an annual basis. Plus, Penman E_p formulation in that form
 515 seems to include the proper drivers to describe E in the boreal forest, as E and E_p are highly correlated
 516 at all sites (R^2 between 0.50 and 0.89, average at 0.72).

517 This above analyses were performed using the simplest energy budget closure adjustment for
 518 E . Indeed, multiplying E by $1/CF$ preserves the Bowen ratio ($H/\lambda E$) for missing fluxes, but studies have
 519 demonstrated that this can induce an overcorrection (*e.g.*, Mauder et al., 2018). Nevertheless, such
 520 variation in the Bowen ratio are probably site-dependent, meaning that the attribution of site-specific

521 proportion of Bowen ratio for missing flux values could increase uncertainties in E . Note that all result-
522 based conclusions in this section remain viable when using E uncorrected for energy imbalance.

523 Precipitation totals presented in this section are also tainted by probable uncertainties related
524 to the common wind-induced undercatch problem, particularly with solid precipitation. However,
525 these uncertainties depend on wind speed, and the latter does not vary much between sites (site-
526 averaged wind speeds are between 1.72 and 3.48 m s⁻¹). Furthermore, differences in wind speed are
527 more related to each site measurement height than actual differing wind regimes. Since every site team
528 was aware of the undercatch problem, every instrument deployment was done following diligent
529 procedures (shielded gauges installed at ground-level in wide forest clearings). Considering these
530 precautions as well as likely similar uncertainties between sites, we believe our results still stand.

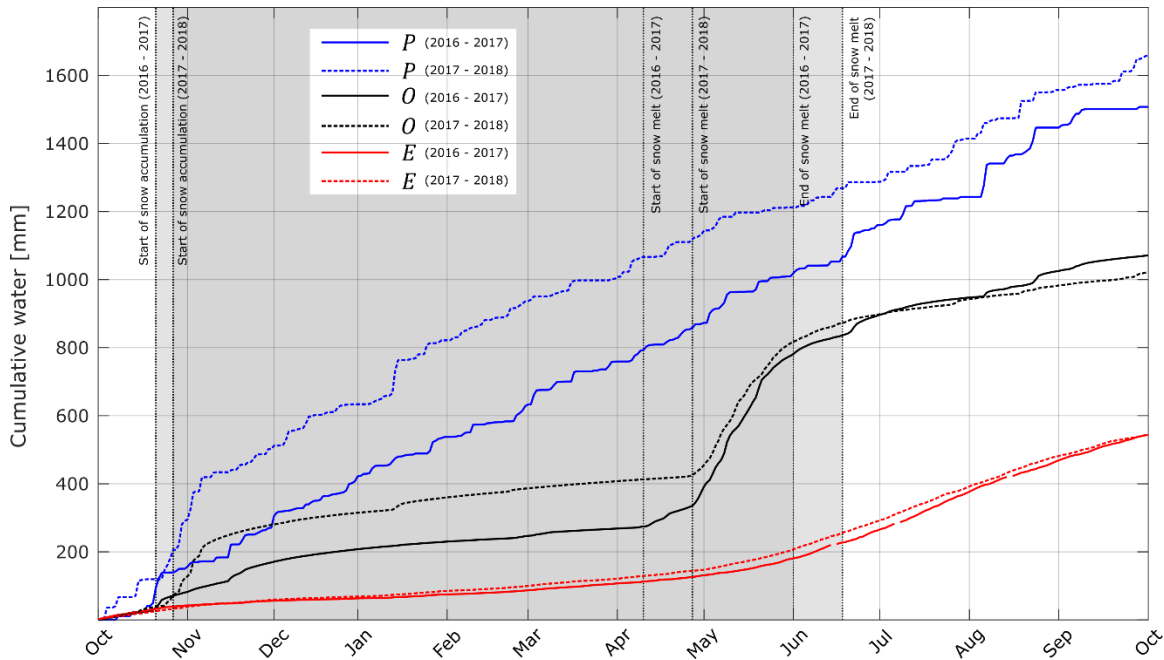
531 Despite the aforementioned limitations, this section has thoroughly demonstrated that the
532 Montmorency Forest is receiving the highest cumulative precipitation of all surveyed sites, by a fair
533 margin. But much higher P does not fully translate into much higher E . To put this in perspective, E
534 values go from 240 mm y⁻¹ (JP2002) to 562 mm y⁻¹ (BF2003), an increase by a factor 2.34, while P
535 values go from 344 mm y⁻¹ (BS1945) to 1444 mm y⁻¹ (BF1993, BF2003), an increase by a factor 4.20.
536 It appears that E has a maximum value (or an upper physical limit), a result observed before in the
537 boreal forest (Brümmer et al., 2012), but not necessarily elsewhere (Zhang et al., 1999). Reasons
538 behind this behaviour could be physiological (ecosystem limit) and/or meteorological (*e.g.*, limited net
539 radiation due to high cloud cover or/and an important atmospheric moisture convergence), but more
540 studies are needed to elucidate this feature. Nevertheless, the Montmorency Forest stand-scale water
541 budget definitely generates an excess of water that can substantially recharge groundwater storage or
542 create strong runoffs.

543

544 5.2. Water allocation of a humid boreal forest

545 The Montmorency Forest sites are ideal to ascertain the effects of high annual precipitation on
546 boreal forest water budgets. Figure 5 presents cumulative curves of every measured water budget
547 components for catchment AB. E is a weighted combination of measurements at the Juvenile and
548 Sapling flux towers ($E_{AB} = (A_A/A_{AB})E_{Juvenile} + (A_B/A_{AB})E_{Sapling}$), where A_A , A_B and A_{AB} are the areas of
549 catchments A, B and AB, respectively). $E_{Juvenile}$ and $E_{Sapling}$ are corrected for non-closure of the energy
550 budget, using CF calculated for the hydrological year (starting in October) and including measurements
551 of G and ΔQ in the available energy estimation. Note that results from measurements taken for sub-
552 catchment A only (not shown) are almost identical to those shown here.

553



554

555 Figure 5: Cumulative precipitation P (blue), evapotranspiration E (red) and watershed outflow O (black) for hydrological years
 556 2016-2017 (full lines) and 2017-2018 (dashed lines) for catchment AB. Hydrological years are defined from October 1 to
 557 September 30 to encompass winter snow-covered periods. The latter periods are illustrated using shades of grey on the graph.

558

559 As it is the case for most boreal watersheds, snow accumulation and melting are highly
 560 impactful on the Montmorency Forest water budget. During the two hydrological years of the study
 561 period, 44% and 33% of the annual precipitation fell in solid state, leading to a maximum seasonal
 562 snowpack depth of 213 cm and 180 cm for 2016-2017 and 2017-2018, respectively. Snowmelt
 563 generates a substantial proportion of annual watershed discharges: 503 mm and 456 mm, or 47% and
 564 45% of total annual discharges in 2016-2017 and 2017-2018, respectively.

565 Throughout both years, E rates were maximized in summer, with 67% and 61% of annual E
 566 occurring from June to September inclusively in 2016-2017 and in 2017-2018, respectively.
 567 Instruments records show that 12% and 16% of annual E occurred as winter sublimation (when air
 568 temperature was below -2°C), in 2016-2017 and 2017-2018, respectively.

569 For both hydrological years, the water budget (Equation 2) did not fully close: subtracting
 570 annual E and O from annual P yielded residuals of -107 mm and 92 mm. These values correspond to
 571 7% and 6% of annual precipitation for 2016-2017 and 2017-2018 respectively. Unfortunately, the
 572 ground water storage part of ΔS was not fully assessed. However, on a hydrological year time scale,
 573 storage variations in soil moisture and snowpack accumulation were not detected. Water table
 574 variations were not measured during the study period, but the small residuals in the water budget
 575 suggest that ground water storage may not vary much from the start of 2016 to the end of 2018.

576 Results need to be put in perspective by stating the uncertainties associated with each
577 measured water budget term. Precipitation measurements are known to be subject to wind-induced
578 undercatch (Kochendorfer et al., 2017). However, the Montmorency Forest is also a site dedicated to
579 study these issues (*e.g.*, Pierre et al., 2019), and the use of DFIR data during winter minimizes
580 uncertainties. Note that when DFIR measurements were available, measured precipitation at the
581 MELCC station accounted for 79% of DFIR measurements, and annual precipitation height increased
582 from 1383 to 1508 mm y⁻¹ and from 1482 to 1659 mm y⁻¹ for 2016-2017 and 2017-2018, respectively.
583 Undercatch is also a problem with liquid precipitation, and can amount to 4-6% (Sevruk et al., 2009).

584 Errors on O are minimal, since rating curve for the weirs have been constructed and verified
585 frequently over 50 years, and include ice-cover periods. Overflow events seldom happen but are
586 accounted for in the rating curves. It is hypothesized that some water flows underground out of the
587 (head) AB watershed, and piezometers have recently been installed to verify underground water
588 movement and storage. E errors are estimated using the random uncertainty method (Finkelstein &
589 Sims, 2001), and they amount to 18% of annual E for each hydrological year (*e.g.*, the variability in
590 Figure 4). Uncertainties also stem from the assumption of spatial representativeness of the flux towers
591 E and the surface-weighted combination method. Watershed E is frequently the greatest source of
592 uncertainties in watershed modeling (Donohue et al., 2010; Seiller & Anctil, 2014).

593 Despite these uncertainties, results paint a clear picture of the watershed. As was concluded
594 in previous studies (*e.g.*, Barr et al., 2012; Brümmer et al., 2012), E rates are capped between 500 and
595 600 mm y⁻¹ even in the presence of high precipitation height and maximum water availability. Excess
596 precipitation then necessarily generates runoff and streamflow or recharge of ground water, which is
597 quite beneficial to the society. Water table recharge is plausible, considering that the immature canopy
598 is unclosed, and hence water reaches and infiltrates the ground easily (Isabelle et al., 2018a). However,
599 given the hilly topography of the site, subsurface flow to streams seems more probable. Nevertheless,
600 it is clear that watershed discharge is the main water-evacuating process in place. This behaviour is
601 typical for a mountainous headwater catchment.

602

603 **6. Conclusion**

604 The balsam fir – white birch stand of the Montmorency Forest vastly stands out as the area
605 receiving the largest annual precipitation amongst all of the 15 studied boreal forested locations. All
606 sites respond to increasing precipitation by generating more E fluxes, but dry environments tend to
607 evaporate a larger proportion of annual precipitation because of higher evaporative demand. The
608 Montmorency Forest thus provides supplemental information that complement the previously
609 available (drier) sites that were used in comparison. E appears to be capped at around 550 mm y⁻¹:
610 this could be a physiological limit of boreal species and climate or because simultaneous increases in

611 P and E_p are unlikely given that precipitation imply cloud cover (hence reduced net radiation), which
612 decreases E_p . More studies partitioning E in its main components (transpiration, ground evaporation,
613 and evaporation of intercepted precipitation) are needed to further our understanding of this
614 observed ecohydrological limit.

615 Using precise measurements of watershed discharges at the Montmorency Forest sites, this
616 study also outlined the watershed-scale (3.6 km²) water budget of two hydrological years in a high-
617 precipitation balsam fir boreal forest. Since E appears to be bounded by a maximum annual value
618 ($\approx 30\%$ of P), excess water mostly becomes water discharge. This behaviour is typical of water budgets
619 of headwater mountainous catchments. Water table measurements are still needed to thoroughly
620 describe the watershed regime, but results are upcoming on this front.

621 To conclude, this study offers a precise experimental description of the catchment
622 hydrological regime of a humid boreal forest typical of northeastern North America. Given the
623 probable climate-change induced increase in precipitation, our results should be taken in
624 consideration by hydroclimate modellers, especially those focused in the boreal zones of the world. In
625 particular, they should expect that increases in precipitation will generate more watershed outflows
626 than evapotranspiration rises.

627

628 **7. Acknowledgments**

629 The authors acknowledge all Montmorency Forest staff, especially Patrick Pineault and
630 Charles Villeneuve, for their extremely valuable help in the field. We also would like to thank Annie-
631 Claude Parent, Dany Crépault, Denis Jobin, Jean-Pierre Tatchegnon Gbegan, Benjamin Bouchard,
632 Sophie Robitaille, Derek Jensen, Chaoxun Hang, Pascale Girard, Martin Pharand, Gabriel Hould
633 Gosselin, Fabien Gaillard Blancard, Marie-Hélène Asselin, Audrey Combes, Bram Hadiwijaya and Achut
634 Parajuli for their help installing the Juvenile and Sapling towers and instrumentation. This work was
635 supported by the Natural Sciences and Engineering Research Council of Canada (NSERC), Ouranos
636 Consortium, Hydro-Québec, Environment and Climate Change Canada, and Ministère de
637 l'Environnement et de la Lutte contre les Changements climatiques (MELCC), through NSERC project
638 RDCPJ-477125-14, and by the the Fonds de recherche du Québec - Nature et Technologies (FRQNT).

639 This work used eddy covariance data acquired and shared by the FLUXNET community,
640 including these networks: AmeriFlux, AfriFlux, AsiaFlux, CarboAfrica, CarboEuropeIP, CarboItaly,
641 CarboMont, ChinaFlux, Fluxnet-Canada, GreenGrass, ICOS, KoFlux, LBA, NECC, OzFlux-TERN, TCOS-
642 Siberia, and USCCC. The ERA-Interim reanalysis data are provided by ECMWF and processed by LSCE.
643 The FLUXNET eddy covariance data processing and harmonization was carried out by the European
644 Fluxes Database Cluster, AmeriFlux Management Project, and Fluxdata project of FLUXNET, with the
645 support of CDIAC and ICOS Ecosystem Thematic Center, and the OzFlux, ChinaFlux and AsiaFlux offices.

646

647 **8. References**

648 Aubinet, M., Chermanne, B., Vandenhaute, M., Longdoz, B., Yernaux, M., & Laitat, E. (2001). Long term
649 carbon dioxide exchange above a mixed forest in the Belgian Ardennes. *Agric. For. Meteorol.*, *108*, 293–
650 315. doi:10.1016/S0168-1923(01)00244-1.

651

652 Baldocchi, D. D., Vogel, C. A., & Hall, B. (1997). Seasonal variation of energy and water vapor exchange
653 rates above and below a boreal jack pine forest canopy. *J. Geophys. Res. Atmos.*, *102*, 28939–28951.
654 doi:10.1029/96JD03325.

655

656 Barber, V. A., Juday, G. P., & Finney, B. P. (2000). Reduced growth of Alaskan white spruce in the
657 twentieth century from temperature-induced drought stress. *Nature*, *405*, 668.
658 doi:10.1038/35015049.

659

660 Barr, A. G., Betts, A. K., Black, T. A., McCaughey, J., & Smith, C. (2001). Intercomparison of BOREAS
661 northern and southern study area surface fluxes in 1994. *J. Geophys. Res. Atmos.*, *106*, 33543–33550.
662 doi:10.1029/2001JD900070.

663

664 Barr, A., Griggs, T., Black, T. A., Lee, X., Staebler, R., Fuentes, J., Chen, Z., & Morgenstern, K. (2002).
665 Comparing the carbon budgets of boreal and temperate deciduous forest stands. *Can. J. For. Res.*, *32*,
666 813–822. doi:10.1139/x01-131.

667

668 Barr, A., Morgenstern, K., Black, T. A., McCaughey, J., & Nestic, Z. (2006). Surface energy balance closure
669 by the eddy-covariance method above three boreal forest stands and implications for the
670 measurement of the CO₂ flux. *Agric. For. Meteorol.*, *140*, 322–337.
671 doi:10.1016/j.agrformet.2006.08.007.

672

673 Barr, A., Van der Kamp, G., Black, T. A., McCaughey, J., & Nestic, Z. (2012). Energy balance closure at the
674 BERMS flux towers in relation to the water balance of the White Gull Creek watershed 1999–2009.
675 *Agric. For. Meteorol.*, *153*, 3–13. doi:10.1016/j.agrformet.2011.05.017.

676

677 Bergeron, O., Margolis, H. A., Black, T. A., Coursolle, C., Dunn, A. L., Barr, A. G., & Wofsy, S. C. (2007).
678 Comparison of carbon dioxide fluxes over three boreal black spruce forests in Canada. *Glob. Change*
679 *Biol.*, *13*, 89–107. doi:10.1111/j.1365-2486.2006.01281.x.

680

681 Blanken, P., Black, T. A., Neumann, H., Den Hartog, G., Yang, P., Nestic, Z., Staebler, R., Chen, W., & Novak,
682 M. (1998). Turbulent flux measurements above and below the overstory of a boreal aspen forest.
683 *Boundary-Layer Meteorol.*, *89*, 109–140. doi:10.1023/A:1001557022310.

684

685 Blanken, P., Black, T. A., Yang, P., Neumann, H., Nestic, Z., Staebler, R., Den Hartog, G., Novak, M., & Lee,
686 X. (1997). Energy balance and canopy conductance of a boreal aspen forest: partitioning overstory and
687 understory components. *J. Geophys. Res. Atmos.*, *102*, 28915–28927. doi:10.1029/97JD00193.

688

689 Brandt, J., Flannigan, M., Maynard, D., Thompson, I., & Volney, W. (2013). An introduction to Canada's
690 boreal zone: ecosystem processes, health, sustainability, and environmental issues. *Environ. Rev.*, *21*,
691 207–226. doi:10.1139/er-2013-0040.

692

693 Brown, S., Petrone, R., Chasmer, L., Mendoza, C., Lazerjan, M., Landhäusser, S., Silins, U., Leach, J., &
694 Devito, K. (2014). Atmospheric and soil moisture controls on evapotranspiration from above and
695 within a Western Boreal Plain aspen forest. *Hydrol. Process.*, *28*, 4449–4462. doi:10.1002/hyp.9879.

696

697 Brümmer, C., Black, T. A., Jassal, R. S., Grant, N. J., Spittlehouse, D. L., Chen, B., Nestic, Z., Amiro, B. D.,
698 Arain, M. A., & Barr, A. G. (2012). How climate and vegetation type influence evapotranspiration and
699 water use efficiency in Canadian forest, peatland and grassland ecosystems. *Agric. For. Meteorol.*, *153*,
700 14–30. doi:10.1016/j.agrformet.2011.04.008.

701

702 Brutsaert, W. (1982). *Evaporation into the Atmosphere: Theory, History, and Applications*. Reidel,
703 Dordrecht, The Netherlands.

704

705 Brutsaert, W. (2005). *Hydrology: an Introduction*. Cambridge University Press, Cambridge, Mass.

706

707 Budyko, M. (1958). *The heat balance of the earth's surface*. Springer, Washington, DC.

708

709 Budyko, M. I. (1974). *Climate and life*. Academic, New York, NY.

710

711 Coursolle, C., Margolis, H. A., Barr, A. G., Black, T. A., Amiro, B. D., Mc-Caughey, J. H., Flanagan, L. B.,
712 Lafleur, P. M., Roulet, N. T., Bourque, C. P.-A. et al. (2006). Late-summer carbon fluxes from Canadian
713 forests and peatlands along an east west continental transect. *Can. J. For. Res.*, *36*, 783–800.
714 doi:10.1139/x05-270.

715

716 Donohue, R. J., McVicar, T. R., & Roderick, M. L. (2010). Assessing the ability of potential evaporation
717 formulations to capture the dynamics in evaporative demand within a changing climate. *J. Hydrol.*, *386*,
718 186–197. doi:10.1016/j.jhydrol.2010.03.020.

719

720 D'Orangeville, L., Duchesne, L., Houle, D., Kneeshaw, D., Côté, B., & Pederson, N. (2016). Northeastern
721 North America as a potential refugium for boreal forests in a warming climate. *Science*, *352*, 1452–
722 1455. doi:10.1126/science.aaf4951.

723

724 Finkelstein, P. L., & Sims, P. F. (2001). Sampling error in eddy correlation flux measurements. *J. Geophys.*
725 *Res.*, *106*, 3503–3509. doi:10.1029/2000JD900731.

726

727 FLUXNET–Canada (2016). *FLUXNET Canada Research Network - Canadian Carbon Program Data*
728 *Collection, 1993-2014*. ORNL DAAC, Oak Ridge, TN. doi:10.3334/ORNLDAAC/1335.

729

730 Foken, T. (2008). The energy balance closure problem: An overview. *Ecol. Appl.*, *18*, 1351–1367.
731 doi:10.1890/06-0922.1.

732

733 Foken, T., Mauder, M., Liebethal, C., Wimmer, F., Beyrich, F., Leps, J.-P., Raasch, S., DeBruin, H. A. R.,
734 Meijninger, W. M. L., & Bange, J. (2010). Energy balance closure for the LITFASS-2003 experiment.
735 *Theor. Appl. Climatol.*, *101*, 149–160.

736

737 Gao, Y., Markkanen, T., Aurela, M., Mammarella, I., Thum, T., Tsuruta, A., Yang, H., Aalto, T. et al. (2017).
738 Response of water use efficiency to summer drought in a boreal Scots pine forest in Finland.
739 *Biogeosciences*, *14*, 4409–4422. doi:10.5194/bg-14-4409-2017.

740

741 Garai, A., Kleissl, J., & Smith, S. G. L. (2010). Estimation of biomass heat storage using thermal infrared
742 imagery: application to a walnut orchard. *Boundary-Layer Meteorol.*, *137*, 333–342.
743 doi:10.1007/s10546-010-9524-x.

744

745 Gauthier, S., Bernier, P., Kuuluvainen, T., Shvidenko, A., & Schepaschenko, D. (2015). Boreal forest
746 health and global change. *Science*, *349*, 819–822. doi:10.1126/science.aaa9092.

747

748 Geissbühler, P., Siegwolf, R., & Eugster, W. (2000). Eddy covariance measurements on mountain slopes:
749 the advantage of surface-normal sensor orientation over a vertical set-up. *Boundary-Layer Meteorol.*,
750 96, 371–392. doi:10.1023/A:1002660521017.

751

752 Gentine, P., D’Odorico, P., Lintner, B. R., Sivandran, G., & Salvucci, G. (2012). Interdependence of climate,
753 soil, and vegetation as constrained by the Budyko curve. *Geophys. Res. Lett.*, 39.
754 doi:10.1029/2012GL053492.

755

756 Giasson, M.-A., Coursolle, C., & Margolis, H. A. (2006). Ecosystem-level CO₂ fluxes from a boreal cutover
757 in eastern Canada before and after scarification. *Agric. For. Meteorol.*, 140, 23–40.
758 doi:10.1016/j.agrformet.2006.08.001.

759

760 Goulden, M., Anderson, R., Bales, R., Kelly, A., Meadows, M., & Winston, G. (2012). Evapotranspiration
761 along an elevation gradient in California’s Sierra Nevada. *J. Geophys. Res. Biogeosci.*, 117.
762 doi:10.1029/2012JG002027.

763

764 Hammerle, A., Haslwanter, A., Schmitt, M., Bahn, M., Tappeiner, U., Cernusca, A., & Wohlfahrt, G. (2007).
765 Eddy covariance measurements of carbon dioxide, latent and sensible energy fluxes above a meadow
766 on a mountain slope. *Boundary-Layer Meteorol.*, 122, 397–416. doi:10.1007/s10546-006-9109-x.

767

768 Hiller, R., Zeeman, M. J., & Eugster, W. (2008). Eddy-covariance flux measurements in the complex
769 terrain of an alpine valley in Switzerland. *BoundaryLayer Meteorol.*, 127, 449–467.
770 doi:10.1007/s10546-008-9267-0.

771

772 Ikawa, H., Nakai, T., Busey, R. C., Kim, Y., Kobayashi, H., Nagai, S., Ueyama, M., Saito, K., Nagano, H.,
773 Suzuki, R. et al. (2015). Understory CO₂, sensible heat, and latent heat fluxes in a black spruce forest in
774 interior Alaska. *Agric. For. Meteorol.*, 214, 80–90. doi:10.1016/j.agrformet.2015.08.247.

775

776 Ilvesniemi, H., Pumpanen, J., Duursma, R., Hari, P., Keronen, P., Kolari, P., Kulmala, M., Mammarella, I.,
777 Nikinmaa, E., Rannik, Ü. et al. (2010). Water balance of a boreal Scots pine forest. *Boreal Environ. Res.*,
778 15, 375–396.

779

780 IPCC (2013). Contribution of working group I to the fifth assessment report of the Intergovernmental
781 Panel on Climate Change. In *Climate Change 2013: The Physical Science Basis*. Cambridge University
782 Press, Cambridge, Mass.

783

784 Isabelle, P.-E., Nadeau, D. F., Asselin, M.-H., Harvey, R., Musselman, K. N., Rousseau, A. N., & Anctil, F.
785 (2018a). Solar radiation transmittance of a boreal balsam fir canopy: Spatiotemporal variability and
786 impacts on growing season hydrology. *Agric. For. Meteorol.*, 263, 1–14. doi:10.1016/j.agrformet.
787 2018.07.022.

788

789 Isabelle, P.-E., Nadeau, D. F., Rousseau, A. N., & Anctil, F. (2018b). Water budget, performance of
790 evapotranspiration formulations, and their impact on hydrological modeling of a small boreal
791 peatland-dominated watershed. *Can. J. Earth Sci.*, 55, 206–220. doi:10.1139/cjes-2017-0046.

792

793 Jarvis, P., Massheder, J., Hale, S., Moncrieff, J., Rayment, M., & Scott, S. (1997). Seasonal variation of
794 carbon dioxide, water vapor, and energy exchanges of a boreal black spruce forest. *J. Geophys. Res.*
795 *Atmos.*, 102, 28953– 28966. doi:10.1029/97JD01176.

796

797 Katul, G. G., & Parlange, M. B. (1992). A Penman-Brutsaert model for wet surface evaporation. *Water*
798 *Resour. Res.*, 28, 121–126. doi:10.1029/91WR02324.

799

800 Kauppi, P. E., Posch, M., & Pirinen, P. (2014). Large impacts of climatic warming on growth of boreal
801 forests since 1960. *PLoS One*, 9, e111340. doi:10.1371/journal.pone.0111340.

802

803 Kochendorfer, J., Rasmussen, R., Wolff, M., Baker, B., Hall, M. E., Meyers, T., Landolt, S., Jachcik, A.,
804 Isaksen, K., Brækkan, R. et al. (2017). The quantification and correction of wind-induced precipitation
805 measurement errors. *Hydrol. Earth Syst. Sci.*, 21, 1973–1989. doi:10.5194/hess-21-1973-2017.

806

807 Kurbatova, J., Li, C., Varlagin, A., Xiao, X., & Vygodskaya, N. (2008). Modeling carbon dynamics in two
808 adjacent spruce forests with different soil conditions in Russia. *Biogeosciences*, 5, 969–980.
809 doi:10.5194/bg-5-969-2008.

810

811 Landsberg, J. J., & Gower, S. T. (1997). *Applications of physiological ecology to forest management*.
812 Academic Press, New York, NY.

813

814 Lavigne, M.-P. (2007). *Modélisation du régime hydrologique et de l'impact des coupes forestières sur*
815 *l'écoulement du ruisseau des Eaux-Volées à l'aide d'HYDROTEL*. Master's thesis, Institut national de la
816 recherche scientifique - Centre Eau Terre Environnement, Québec, Canada.

817

818 Leuning, R., Van Gorsel, E., Massman, W. J., & Isaac, P. R. (2012). Reflections on the surface energy
819 imbalance problem. *Agric. For. Meteorol.*, 156, 65-74. doi:10.1016/j.agrformet.2011.12.002.
820

821 Liu, P., Black, T. A., Jassal, R. S., Zha, T., Nestic, Z., Barr, A. G., Helgason, W. D., Jia, X., Tian, Y., Stephens, J.
822 J. et al. (2019). Divergent long-term trends and interannual variation in ecosystem resource use
823 efficiencies of a southern boreal old black spruce forest 1999–2017. *Glob. Change Biol.*
824 doi:10.1111/gcb.14674.
825

826 Lloyd, A. H., & Bunn, A. G. (2007). Responses of the circumpolar boreal forest to 20th century climate
827 variability. *Environ. Res. Lett.*, 2, 045013. doi:10.1088/1748-9326/2/4/045013.
828

829 Mauder, M., & Foken, T. (2011). *Documentation and instruction manual of the eddy-covariance software*
830 *package TK3*. Technical Report, Universität Bayreuth, Germany.
831

832 Mauder, M., Genzel, S., Fu, J., Kiese, R., Soltani, M., Steinbrecher, R., Zeeman, M., Banerjee, T., De Roo, F.,
833 & Kunstmann, H. (2018). Evaluation of energy balance closure adjustment methods by independent
834 evapotranspiration estimates from lysimeters and hydrological simulations. *Hydrol. Process.*, 32, 39–
835 50. doi:10.1002/hyp.11397.
836

837 McCaughey, J. H. (1978). Energy balance and evapotranspiration estimates for a mature coniferous
838 forest. *Can. J. For. Res.*, 8(4), 456-462. doi:10.1139/x78-067.
839

840 McCaughey, J., Pejam, M., Arain, M., & Cameron, D. (2006). Carbon dioxide and energy fluxes from a
841 boreal mixedwood forest ecosystem in Ontario, Canada. *Agric. For. Meteorol.*, 140, 79–96.
842 doi:10.1016/j.agrformet.2006.08.010.
843

844 MELCC (2019). *Données du programme de surveillance du climat*. Direction générale de la surveillance
845 du climat, Ministère de l'Environnement et de la Lutte contre les Changements Climatiques, Québec,
846 Canada.
847

848 Mkhabela, M., Amiro, B., Barr, A., Black, T. A., Hawthorne, I., Kidston, J., McCaughey, J., Orchansky, A.,
849 Nestic, Z., Sass, A., Shashkov, A., & Zhab, T. (2009). Comparison of carbon dynamics and water use
850 efficiency following fire and harvesting in Canadian boreal forests. *Agric. For. Meteorol.*, 149, 783–794.
851 doi:10.1016/j.agrformet.2008.10.025.
852

853 Moffat, A. M., Papale, D., Reichstein, M., Hollinger, D. Y., Richardson, A. D., Barr, A. G., Beckstein, C.,
854 Braswell, B. H., Churkina, G., & Desai, A. R. (2007). Comprehensive comparison of gap-filling techniques
855 for eddy covariance net carbon fluxes. *Agric. For. Meteorol.*, *147*, 209–232.

856

857 Moncrieff, J., Clement, R., Finnigan, J., & Meyers, T. (2004). Averaging, detrending, and filtering of eddy
858 covariance time series. In X. Lee, W. Massman, & B. Law (Eds.), *Handbook of micrometeorology: a guide*
859 *for surface flux measurement and analysis* (pp. 7–31). Springer, Dordrecht, The Netherlands.

860

861 Moncrieff, J. B., Massheder, J., De Bruin, H., Elbers, J., Friborg, T., Heusinkveld, B., Kabat, P., Scott, S.,
862 Sørensen, H., & Verhoef, A. (1997). A system to measure surface fluxes of momentum, sensible heat,
863 water vapour and carbon dioxide. *J. Hydrol.*, *188*, 589–611.

864

865 Nadeau, D. F., Pardyjak, E. R., Higgins, C. W., Huwald, H., & Parlange, M. B. (2013a). Flow during the
866 evening transition over steep alpine slopes. *Q. J. R. Meteorol. Soc.*, *139*, 607–624. doi:10.1002/qj.1985.

867 Nadeau, D. F., Pardyjak, E. R., Higgins, C. W., & Parlange, M. B. (2013b). Similarity scaling over a steep
868 alpine slope. *Boundary-Layer Meteorol.*, *147*, 401–419. doi:10.1007/s10546-012-9787-5.

869

870 Nijssen, B., & Lettenmaier, D. P. (2002). Water balance dynamics of a boreal forest watershed: White
871 Gull Creek basin, 1994–1996. *Water Resour. Res.*, *38*. doi:10.1029/2001WR000699.

872

873 Noël, P., Rousseau, A. N., Paniconi, C., & Nadeau, D. F. (2014). Algorithm for delineating and extracting
874 hillslopes and hillslope width functions from gridded elevation data. *J. Hydrol. Eng.*, *19*, 366–374.
875 doi:10.1061/(ASCE)HE.1943-5584.0000783.

876

877 Ochsner, T. E., Sauer, T. J., & Horton, R. (2007). Soil heat storage measurements in energy balance
878 studies. *Agron. J.*, *99*, 311–319. doi:10.2134/agronj2005.0103S.

879

880 Oldroyd, H. J., Pardyjak, E. R., Huwald, H., & Parlange, M. B. (2016). Adapting tilt corrections and the
881 governing flow equations for steep, fully three-dimensional, mountainous terrain. *Boundary-Layer*
882 *Meteorol.*, *159*, 539–565. doi:10.1007/s10546-015-0066-0.

883

884 Oliphant, A., Grimmond, C., Zutter, H., Schmid, H., Su, H.-B., Scott, S., Offerle, B., Randolph, J., & Ehman,
885 J. (2004). Heat storage and energy balance fluxes for a temperate deciduous forest. *Agric. For. Meteorol.*,
886 *126*, 185–201. doi:10.1016/j.agrformet.2004.07.003.

887

888 Oltchev, A., Cermak, J., Gurtz, J., Tishenko, A., Kiely, G., Nadezhdina, N., Zappa, M., Lebedeva, N., Vitvar,
889 T., Albertson, J. et al. (2002). The response of the water fluxes of the boreal forest region at the Volga's
890 source area to climatic and land-use changes. *Phys. Chem. Earth Pt A/B/C*, 27, 675–690.
891 doi:10.1016/S1474-7065(02)00052-9.

892

893 Ono, K., Mano, M., Miyata, A., & Inoue, Y. (2008). Applicability of the planar fit technique in estimating
894 surface fluxes over flat terrain using eddy covariance. *J. Agric. Meteorol. (Jpn)*, 64, 121–130.

895

896 Pan, Y., Birdsey, R. A., Fang, J., Houghton, R., Kauppi, P. E., Kurz, W. A., Phillips, O. L., Shvidenko, A., Lewis,
897 S. L., Canadell, J. G., Ciais, P., Jackson, R. B., Pacala, S., McGuire, A. D., Piao, S., Rautiainen, A., Sitch, S., &
898 Hayes, D. (2011). A large and persistent carbon sink in the world's forests. *Science*, 333, 988–993.
899 doi:10.1126/science.1201609.

900

901 Papale, D., Reichstein, M., Aubinet, M., Canfora, E., Bernhofer, C., Kutsch, W., Longdoz, B., Rambal, S.,
902 Valentini, R., Vesala, T. et al. (2006). Towards a standardized processing of Net Ecosystem Exchange
903 measured with eddy covariance technique: algorithms and uncertainty estimation. *Biogeosciences*, 3,
904 571–583.

905

906 Papale, D., & Valentini, R. (2003). A new assessment of European forests carbon exchanges by eddy
907 fluxes and artificial neural network spatialization. *Glob. Change Biol.*, 9, 525–535. doi:10.1046/j.1365-
908 2486.2003.00609.x.

909

910 Pastorello, G., Agarwal, D., Papale, D., Samak, T., Trotta, C., Ribeca, A., Poindexter, C., Faybishenko, B.,
911 Gunter, D., Hollowgrass, R. et al. (2014). Observational data patterns for time series data quality
912 assessment. In *2014 IEEE 10th International Conference on e-Science* (pp. 271–278). IEEE volume 1.

913

914 Payeur-Poirier, J.-L., Coursolle, C., Margolis, H. A., & Giasson, M.-A. (2012). CO₂ fluxes of a boreal black
915 spruce chronosequence in eastern North America. *Agric. For. Meteorol.*, 153, 94–105.
916 doi:10.1016/j.agrformet.2011.07.009.

917

918 Penman, H. L. (1948). Natural evaporation from open water, bare soil and grass. *Proc. R. Soc. Lond.*,
919 A193, 120–145.

920

921 Pierre, A., Jutras, S., Smith, C., Kochendorfer, J., Fortin, V., & Anctil, F. (2019). Evaluation of catch
922 efficiency transfer functions for unshielded and single-Alter-shielded solid precipitation
923 measurements. *J. Atmos. Ocean. Tech.* doi:10.1175/JTECH-D-18-0112.1.
924

925 Reichstein, M., Falge, E., Baldocchi, D., Papale, D., Aubinet, M., Berbigier, P., Bernhofer, C., Buchmann,
926 N., Gilmanov, T., & Granier, A. (2005). On the separation of net ecosystem exchange into assimilation
927 and ecosystem respiration: review and improved algorithm. *Glob. Change Biol.*, 11, 1424– 1439.
928 doi:10.1111/j.1365-2486.2005.001002.x.
929

930 Saugier, B., Granier, A., Pontauiller, J., Dufrene, E., & Baldocchi, D. (1997). Transpiration of a boreal pine
931 forest measured by branch bag, sap flow and micrometeorological methods. *Tree Physiol.*, 17, 511–519.
932 doi:10.1093/treephys/17.8-9.511.
933

934 Schaphoff, S., Reyer, C. P., Schepaschenko, D., Gerten, D., & Shvidenko, A. (2016). Tamm Review:
935 Observed and projected climate change impacts on Russia’s forests and its carbon balance. *Forest Ecol.*
936 *Manag.*, 361, 432–444. doi:10.1016/j.foreco.2015.11.043.
937

938 Seiller, G., & Anctil, F. (2014). Climate change impacts on the hydrologic regime of a Canadian river:
939 comparing uncertainties arising from climate natural variability and lumped hydrological model
940 structures. *Hydrol. Earth Syst. Sci.*, 18, 2033–2047. doi:10.5194/hess-18-2033-2014.
941

942 Sellers, P., Hall, F., Margolis, H., Kelly, B., Baldocchi, D., den Hartog, G., Cihlar, J., Ryan, M. G., Goodison,
943 B., Crill, P. et al. (1995). The Boreal Ecosystem–Atmosphere Study (BOREAS): an overview and early
944 results from the 1994 field year. *Bull. Am. Meteorol. Soc.*, 76, 1549–1577. doi:10.1175/1520-
945 0477(1995)076<1549:TBESAO>2.0.CO;2.
946

947 Sellers, P. J., Hall, F. G., Kelly, R. D., Black, T. A., Baldocchi, D., Berry, J., Ryan, M., Ranson, K. J., Crill, P. M.,
948 Lettenmaier, D. P. et al. (1997). BOREAS in 1997: Experiment overview, scientific results, and future
949 directions. *J. Geophys. Res. Atmos.*, 102, 28731–28769. doi:10.1029/97JD03300.
950

951 Serrano-Ortiz, P., Sánchez-Cañete, E., Olmo, F., Metzger, S., Pérez-Priego, O., Carrara, A., Alados-
952 Arboledas, L., & Kowalski, A. (2016). Surface-parallel sensor orientation for assessing energy balance
953 components on mountain slopes. *Boundary-Layer Meteorol.*, 158, 489-499. doi:10.1007/s10546-015-
954 0099-4.
955

956 Sevruk, B., Ondras, M., & Chvíla, B. (2009). The WMO precipitation measurement intercomparisons.
957 *Atmos. Res.*, *92*, 376–380. doi:10.1016/j.atmosres.2009.01.016.
958
959 Stiperski, I., & Rotach, M. W. (2016). On the measurement of turbulence over complex mountainous
960 terrain. *Boundary-Layer Meteorol.*, *159*, 97–121. doi:10.1007/s10546-015-0103-z.
961
962 Stoy, P. C., Mauder, M., Foken, T., Marcolla, B., Boegh, E., Ibrom, A., Arain, M.A., Arneth, A., Aurela, M.,
963 Bernhofer, C. & Cescatti, A., (2013). A data-driven analysis of energy balance closure across FLUXNET
964 research sites: The role of landscape scale heterogeneity. *Agric. For. Meteorol.*, *171*, 137-152.
965 doi:10.1016/j.agrformet.2012.11.004.
966
967 Suni, T., Rinne, J., Reissell, A., Altimir, N., Keronen, P., Rannik, U., Maso, M., Kulmala, M., & Vesala, T.
968 (2003). Long-term measurements of surface fluxes above a Scots pine forest in Hyytiälä, southern
969 Finland, 1996-2001. *Boreal Environ. Res.*, *8*, 287–302.
970
971 Ter-Mikaelian, M. T., & Korzukhin, M. D. (1997). Biomass equations for sixty-five North American tree
972 species. *For. Ecol. Manage.*, *97*, 1-24. doi:10.1016/S0378-1127(97)00019-4.
973
974 Thum, T., Aalto, T., Laurila, T., Aurela, M., Kolari, P., & Hari, P. (2007). Parametrization of two
975 photosynthesis models at the canopy scale in a northern boreal Scots pine forest. *Tellus B*, *59*, 874–
976 890. doi:10.1111/j.1600-0889.2007.00305.x.
977
978 Tremblay, Y., Rousseau, A. N., Plamondon, A. P., Levesque, D., & Jutras, S. (2008). Rainfall peak flow
979 response to clearcutting 50% of three small watersheds in a boreal forest, Montmorency Forest,
980 Quebec. *J. Hydrol.*, *352*, 67–76.
981
982 Tremblay, Y., Rousseau, A. N., Plamondon, A. P., Lévesque, D., & Prévost, M. (2009). Changes in stream
983 water quality due to logging of the boreal forest in the Montmorency Forest, Quebec. *Hydrol. Process.*,
984 *23*, 764–776. doi:10.1002/hyp.7175.
985
986 Turnipseed, A., Blanken, P., Anderson, D., & Monson, R. K. (2002). Energy budget above a high-elevation
987 subalpine forest in complex topography. *Agric. For. Meteorol.*, *110*, 177–201. doi:10.1016/S0168-
988 1923(01)00290-8.
989

990 Twine, T. E., Kustas, W., Norman, J., Cook, D., Houser, P., Meyers, T., Prueger, J., Starks, P., & Wesely, M.
991 (2000). Correcting eddy-covariance flux underestimates over a grassland. *Agric. For. Meteorol.*, *103*,
992 279–300. doi:10.1016/S0168-1923(00)00123-4.
993
994 USDA (2007). *The Encyclopedia of Wood*. U.S. Department of Agriculture, Skyhorse Publishing Inc. New
995 York, NY.
996
997 Van Wijk, W. (1963). *Physics of Plant Environment*. North Holland Publishing Co., Amsterdam,
998 Denmark.
999
1000 Vickers, D., & Mahrt, L. (1997). Quality control and flux sampling problems for tower and aircraft data.
1001 *J. Atmos. Ocean. Tech.*, *14*, 512–526.
1002
1003 Vuichard, N., & Papale, D. (2015). Filling the gaps in meteorological continuous data measured at
1004 FLUXNET sites with ERA-Interim reanalysis. *Earth Syst. Sci. Dat.*, *7*, 157–171. doi:10.5194/essd-7-157-
1005 2015.
1006
1007 Walker, X. J., Mack, M. C., & Johnstone, J. F. (2015). Stable carbon isotope analysis reveals widespread
1008 drought stress in boreal black spruce forests. *Glob. Change Biol.*, *21*, 3102–3113.
1009 doi:10.1111/gcb.12893.
1010
1011 Webb, E. K., Pearman, G. I., & Leuning, R. (1980). Correction of flux measurements for density effects
1012 due to heat and water vapour transfer. *Q. J. R. Meteorol. Soc.*, *106*, 85–100.
1013
1014 Whiteman, C. D., & Allwine, K. J. (1986). Extraterrestrial solar radiation on inclined surfaces. *Environ.*
1015 *Soft.*, *1*, 164–169.
1016
1017 Wilczak, J. M., Oncley, S. P., & Stage, S. A. (2001). Sonic anemometer tilt correction algorithms.
1018 *Boundary-Layer Meteorol.*, *99*, 127–150. doi:10.1023/A:1018966204465.
1019
1020 Wohlfahrt, G., Irschick, C., Thalinger, B., Hörtnagl, L., Obojes, N., & Hammerle, A. (2010). Insights from
1021 independent evapotranspiration estimates for closing the energy balance: a grassland case study.
1022 *Vadose Zone J.*, *9*, 1025–1033. doi:10.2136/vzj2009.0158.
1023
1024 Yang, D. (2014). Double fence intercomparison reference (DFIR) vs. bush gauge for “true” snowfall
measurement. *J. Hydrol.*, *509*, 94–100. doi:10.1016/j.jhydrol.2013.08.052.

1025

1026 Zha, T., Barr, A. G., van der Kamp, G., Black, T. A., McCaughey, J. H., & Flanagan, L. B. (2010). Interannual
1027 variation of evapotranspiration from forest and grassland ecosystems in western Canada in relation to
1028 drought. *Agric. For. Meteorol.*, *150*, 1476–1484. doi:10.1016/j.agrformet.2010.08.003.

1029

1030 Zhang, L., Walker, G. R., & Dawes, W. (1999). *Predicting the effect of vegetation changes on catchment*
1031 *average water balance*. Technical Report 99/12 Cooperative Research Center for Catchment
1032 Hydrology, CSIRO Land and Water, Canberra, Australia.